This is a post-peer-review, pre-copyedit version of an article published in **Self-standing Substrates. Engineering Materials**. The final authenticated version is available online at: https://doi.org/10.1007/978-3-030-29522-6_1

Postprint of: Siuzdak K., Haryński Ł., Wawrzyniak J., Kupracz P., Grochowska K., Self-standing Nanoarchitectures. In: Inamuddin, Boddula R., Asiri A. (eds) Self-standing Substrates. Engineering Materials, pp. 1-56 (2020), Springer, https://doi.org/10.1007/978-3-030-29522-6_1

Chapter: Self-standing nanoarchitectures

Katarzyna Siuzdak, Łukasz Haryński, Jakub Wawrzyniak, Piotr Kupracz, Katarzyna Grochowska

Abstract

Despite there are structures invisible for the human eye, they mastered the world of advanced electronic devices, sensors, novel cosmetics or drugs. When the dimensions of the materials go down to the nanometres scale, their properties change dramatically comparing to the observable objects. Because of their tiny size, they gained the name of nanomaterials but simultaneously their importance has significantly grown up. Nanomaterials exhibit superb features such as a distinctive catalytic activity, hydrophobicity, photoconversion activity and biological affinity. Following that, even a small amount of nanomaterials is sufficient to provide unusual properties to the final products such as coatings, active layers in solar cells, clothes, electrodes and electrolytes used for energy storage devices. Owing to the rapid development in the synthesis methods and characterization techniques, especially those used for morphology inspection, we can investigate them in details on the molecular scale and describe the mechanism that stays behind improved antimicrobiological activity, hydrophobicity, capacitance or catalytic properties. Despite the number of usable elements is limited, the diversity of morphologies, namely rods, particles, tubes, planes and the possibility of heterostructures formation, provides researchers the wide room for maneuverer. Sometimes, only small change in the material geometry, structure or a little amount of introduced dopant atoms is enough to obtain completely new nanomaterial that has not been known so far. Therefore, we should not be surprised how fast surrounding environment is changing and our everyday life is supported by the novelties from the nano world.

The aim of this chapter is to present the diversity of nanomaterials taking into account their dimensions, shape and composition. Herein, particles, tubes, wires, pores, walls, exhibiting at least one dimension within the nanoscale will be evoked. Moreover, the nanostructures that morphology reminds well known objects from nature are discussed. The description of some interesting examples is supported by the extraordinary SEM images illustrating the beauty unavailable for naked eye.

1 Introduction

In the present world, more and more electronic devices that plays important role in our life owns its popularity to achievements in nanotechnology: new functional materials, advanced fabrication and characterization techniques. As we need long lasting batteries in our cell phones, highly sensitive diagnostic tests or clothes highly resistant for dirt or moisture, we have to appreciate researchers' efforts to control dimensions, shape and properties of tiny structures. Taking into account such small dimensins, the prefix "nano" originating from the Greek nomenclature and meaning dwarf has been reserved for those objects. Considering nanostructures, we should be aware that at least one of their dimension does not exceed 100 nm and because of that, their morphology cannot by simply verified by visual observation. To realize how small are these structures, the dimensions of selected objects are given in Fig. 1. This diagram illustrates in dimensional scale how nanomaterials are far from those we can just catch in our hands.

Apart from the size, comparing to typical bulk materials, like the silver plate or plastic spoon, nanomaterials exhibit unique physical and chemical properties. Those

size-dependent features, like higher conductivity, degradation of organic pollution, ability to transport small drug molecules or anti-corrosion resistance, justify the importance of intense research in this field. Those nanostructures can be formed directly on the stable substrate, suspended freely in some liquid or may form the powder. Following the way how the nanomaterial is stored, one may distinguish free-standing or substrate bound nanomaterials. In the case of free-standing nanostructures, usually their larger amount looks like a powder and in such form it is stored in the closed container and offered to the customer. However, since the powder is composed of tiny particles, there is a fear of dusting that could be harmful to human health. Because of safety issues, some nanomaterials are stored as a suspension in a liquid medium, usually water or alcohol. The safest form of nanomaterials storage and further transport is their immobilization or in the best case, application of such synthesis method allowing its formation already on the stable substrate. Nevertheless, today optimism towards unique features of nanomaterials and their application in many fields should be balanced by their safe usage, storage and finally recycling.

1.1 Dimensions of nanomaterials

Among variety of materials for which at least one dimension does not exceed 100 nm, one may distinguish four classes: zero (0-D), one (1-D), two (2-D) and three (3-D) – dimensional structures (Tiwari et al., 2012) . Such classification was proposed by Pokropivny and Skotokhod (2007) and Table 1 goes along with his scheme.
However, irrespective of the dimensions, among those structures, we can distinguish amorphous or crystalline, single crystalline or polycrystalline, chemical pure or doped in bulk or only on the surface, standalone materials or embedded within other medium. Nanostructures can be built of metallic or semiconducting units as well as polymeric molecules.

Zero-dimensional nanostructures exhibit all three dimensions in nanometres regime and have a diameter less than 100 nm. Here, we can find nanoclusters possessing irregular structure and dimensions within 1-10 nm range. As nanocrystals, monocrystalline nanostructures are defined with size from 1 to 30 nm. Commonly recognized quantum dots are semiconducting nanocrystals. Recently, apart from the quantum dots, hollow spheres, nanolenses or onion like structures are associated to 0-D group.
For **one-dimensional nanomaterial**, one dimension is outside the nanoscale range. Following that, one can find nanotubes, nanorods and nanowires, nanobelts or even nanoribbons. Nanowires exhibit elongated structures and are obtained from various metallic, semiconducting or oxide materials. They are especially applied in electronics, new generation of photovoltaic devices and sensing platforms. On the contrary, tubular structures possess a hollow interior. The most known tubes are of course carbon structures: single-, double- and multi-walled carbon nanotubes. However, recently the focus is put onto the semiconducting tubular materials, like titania or alumina nanotubes that could be easily formed during anodization.
Two-dimensional nanomaterials exhibit plate-like shape and therefore very thin layers or coatings are there included as well as some disc-like structures. However, their thickness still does not exceed 100 nm. Within 2-D nanostructures one can find branched structures, nanoplates, nanosheets or nanowalls. The most common example of 2-D is graphene due to the unique properties allowing application in different areas, from electronic devices to medicine as the crucial component of sensing electrode material. Additionally, owing to the sophisticated deposition

techniques, like magnetron sputtering, chemical vapour deposition, laser ablation, precisely controlled nanofilm can be formed using targets or chemical compounds as precursors.

Three-dimensional nanomaterials are materials that are not exactly fitting nanoscale at any dimension. Nevertheless, they still have high surface area and provide many adsorption sites for all involved molecules. Within this group bulk powders, dispersion of nanoparticles or some multilayers, polycrystals and bundles of nanotubes or nanowires, nanoballs formed out of dendric structures, nanopillars and nanoflowers are included.

Apart from the dimension factor, nanomaterials can be formed by one or more components leading to the formation of composite. Those counterparts exhibit different properties but can act together in synergy to create features that are not achieved by each single part. The matrix of nanocomposite can be similar to other single materials composed of metal oxides, polymers, metals, ceramics or could state as a mixture of them, e.g. polymer with embedded metal nanoparticles or semiconductor modified with metal nanoparticles. Their dimensions could fit nanoscale range but could also be above them, whereas the reinforcing phase fits the nanoscale range. There, of course, exists several classifications of nanocomposites and following that we can find composites: a) reinforced with discrete particles, b) with interpenetrating skeletons of two or more structural components, c) reinforced with discrete fibres or whiskers, d) reinforced with continuous fibres or e) with layered structures (Khan et al. 2017)

1.2 Difference between nanostructures and bulk structures

As was mentioned at the beginning of this chapter, nanomaterial and the bulk one formed by the same element exhibit totally different features that are caused by increasing relative surface area and quantum effects. As the size decreases, many more atoms forming the particular particle are in direct contact with an outer environment and less and less stay in its core. Taking into account sphere shape, when the particle has only 3 nm in diameter, half of its atoms are on the surface and a half form the core. Therefore, regarding chemical reactions that take place at the materials surface, much higher reactivity could be expected for those tiny structures than for larger parts, assuming that the volume remains the same. Along with the enlarged real surface area, quantum effects control materials properties. They influence optical, magnetic, electrical properties, ability to adsorb certain molecules onto the surface or to inhibit the growth of the bacteria or yeast, known as an interaction with biological creatures. For example, in macroscale, bulk gold is malleable and exhibits beautiful gloss typical for metals. However, when it comes to nanoscale, few nanometres small gold particles could form pink, red or purple colloids depending on the shape and tiny dimensions and because of the size the term malleability loses its importance.

1.3 Fabrication methods

Some of nanomaterials can be found in the natural environment, but in the centre of interest are those that could be designed and fabricated firstly in the laboratory and then easily scaled up to the commercial scale. Fabrication of self-standing nanostructures requires utilization of methods that enable controlled connection of single molecules, ions in bigger structures or fragmentation of solid material into much smaller species. According to those different attempts, two main approaches were proposed: bottom-up and top-down. As indicated in Fig. 2, bottom-up route concerns processes where small components of atomic or molecular dimensions are

put together owing to the natural physical principle or an externally applied force, to obtain complex system. In the case of top-down route, as a substrate, some large piece of material is used and the application of appropriate tools leads to its destruction into smaller components. Within those two approaches one can find various methods that were listed in Table 2 and 3.
Other classification concerns the type of synthesis used for material fabrication, namely physical and chemical approaches could be distinguished. The most frequently used fabrication routes are assigned to each brand and listed in Table 4. Unfortunately, because of high cost of precursors or equipment and the complex preparation route, not all of mentioned techniques can be applied on the commercial scale. Nevertheless, upon intensive research and optimization of fabrication methods, more and more approaches used in the laboratory are moving to the large scale industry. Owing it to the fact that the control of the scaling-up process has been mastered and wide access to the knowledge is assured, the fabrication of nanomaterials comes out from the laboratories and as a result we can find nanostructures in cosmetics, drugs, bandages or household chemicals.

1.4 How to look at nanostructures?

Since nanomaterials are characterized by dimensions at least one thousand times smaller than the diameter of human hair, our eyes or simple optical microscopes are insufficient to observe unique features of their morphology. Thus, special equipment has to be used to get the information about the topography and to obtain information concerning detailed dimensions and shape of nanostructure. For this purpose, advanced microscopes are used, i.e. scanning electron microscope (SEM), transmission electron microscope (TEM) and atomic force microscope (AFM). The enormous progress also in the characterization techniques, leads to the miniaturization of those pieces of laboratory equipment and in the case of AFM and SEM, only a simple office desk is needed for their installation. Despite much lower size of modern microscopes comparing to older ones, the operation principle is preserved and below some short description is given.
Scanning electron microscopy uses the focused flux of high-energy electrons that interacts with the surface and as a result generates variety of signals at the surface of the solid specimen (see Fig. 3a). Those signals are attributed among others to the secondary electrons, backscattered electrons and characteristic X-rays. When electrons meet the surface of the material, they penetrate the sample down to few μm, depending on the optimized parameters such as accelerating voltage and sample density. Different types of generated electrons provide information about the sample including its morphology, chemical composition and even crystalline structure that is regarded as a basic knowledge on the investigated material. Usually, data is collected from the specified area of the sample and converted into two-dimensional image that looks like a black-white photo. As currently advanced optical microscope enables 1500 magnification of the sample, SEM microscope allows even for 500 000 magnification and spatial resolution lower than 1 nm can be achieved. Owing to the additional guns and particular energy recorded in selected place of the investigated samples, information concerning elemental composition using energy dispersive spectroscopy (EDS), crystalline structure or crystal orientation may be obtained. First SEM was constructed by a German technician Max Knoll in 1935, whilst the microscope was offered as a commercial product in 1965. Since time when SEM had been introduced to the laboratories, its dimensions have decreased significantly and some models require only office desk. Moreover, due to the

simplification of the software the special operator is not required and almost everyone after short training can operate SEM.
Despite SEM technique allows to obtain very detailed images of the surface of nanostructures, transmission electron microscopy enables to look even deeper. In general, the construction of both microscopes is similar. However, in the case of TEM, transmitted electrons are analysed and thus the investigated sample has to be semi-transparent to the focused electron flux (see Fig. 3b). For this purpose, nanostructures are deposited onto the special copper grid that is placed in the way of the electron beam. On the contrary to SEM, TEM inspection provides information concerning internal composition covering crystalline or magnetic domains. Moreover, dislocations, tiny precipitates, grain boundaries or even defects could be illustrated. Nevertheless, transmission electron microscopy still requires a lot of space and a highly trained operator.
Other frequently used technique for morphology investigation is atomic force microscopy. This approach was initially used to visualise surface with atomic scale resolution. The operation principle of AFM is based on recording the modulation of the topographical signal originating from the interaction between materials surface and a very sensitive position detector. The role of this detector is played by the tiny cantilever looking as a needle with an extremely sharp tip at its end. The tip being of tens of nanometres in its dimension scans horizontally the surface of the material. During those scans, the position of cantilever is measured by the system composed of laser beam that is collimated onto the arm, as indicated in Fig. 3c, and reflected light is captured at diode detector. AFM imaging also provides information about the materials' topography in nm-rage, however in the investigated area, the difference between some spots cannot be too high as that lowers image quality. AFM was constructed in 1986 by the team of G. Binning, C.F. Quate and C. Gerner. Their works were forced by the SEM limitations, since isolator cannot be observed under electron microscope. Now, owing to the great improvements concerning AFM technique, sample investigation could be performed even on living cells in their natural liquid environment. As was in the case of SEM, AFM microscopes have become popular and are used as a typical equipment for students laboratory lessons whereas in industry allow for control of optical materials, semiconductors or data storages.
Summarizing, the material imaging inseparably accompanies the fabrication of nanostructures to confirm their size, expected morphology that affects the physicochemical features and in consequence future application areas. Fortunately, some new technical solutions, additional detectors or upgraded software allow to gain information also about crystal phase, magnetic character or elemental composition.

2 Nanoparticles

As has been already defined, nanoparticles (NPs) are a tiny pieces of matter which are usually between 1 and 100 nanometres in size, thus they are sometimes referred to as zero-dimensional (0-D) materials. Nanoparticles are often best described by their material, size and morphology (see Fig. 4), but different classification criteria are sometimes used in literature depending on the synthesis methods or their functionalization.
Extraordinary properties of the nanoparticles origin from their high surface-to-volume ratio. Because of high reactivity, nanoparticles could bind to each other in their immediate vicinity. This particular feature could be regarded either as an advantage or disadvantage, depending on their particular application. In order to

prevent agglomeration, their surface is often modified with the surface active agents, resulting in attenuation of chemical activity, whereas their physical properties are preserved. Similarly, nanoparticles can be functionalized using certain functional groups immobilized onto their surface (Gangadoo et al. 2017).

2.1 Noble metal nanoparticles

Among others, metal nanoparticles, especially noble metal NPs, are the most broadly applied ones. They can be synthesized by variety of techniques and their size and shape can be easily tailored by choosing an adequate synthesis method. Owing to the free electrons present in metal nanoparticles, most of them exhibit clear absorbance bands within the visible waverange. Thanks to their uniform surface chemistry, they are also regarded as great candidates for functionalization, extending the field of potential application even further.

Concerning noble NPs, gold nanoparticles (see Fig. 5 a) are extensively investigated. They can be synthesized via bottom-up and top-down approaches, but in most cases, the reduction of chloroauric acid ($HAuCl_4$) is utilized for their fabrication. In a simple reaction we can obtain gold NPs exhibiting a perfect spherical shape. However, rapid agglomeration without the addition of surface capping agents, e.g. cetrimonium bromide (CTAB), may result in inhibition of their beneficial properties, namely surface enhanced Raman spectroscopy (SERS) emission (Benz et al. 2016).

In order to develop more distinctive surface morphologies, additional weak reducing agent along with metal ions, particularly Ag^+, might be added, which can selectively passivate surface of the nanoparticle. Following that procedure, at varying ions and nanoparticles ratios, one can produce different NPs shapes like triangles, bipyramids or stars (see Fig. 5 b, c) affecting their physicochemical features (Kuttner et al. 2018, Jiji and Gopchandran 2015).

Very similarly to gold NPs, platinum nanoparticles can be synthesized. By adding sodium citrate and citric acid to boiling, aqueous solution containing chloroplatinic acid hexahydrate, we can initiate precipitation of Pt nanostructures and finally NPs of about 5 nm in diameter are formed (Bigall et al. 2008). Those tiny particles can then be used as seeds for further particle growth, opening up further possibilities to develop their size and form.

2.2 Core-shell type nanoparticles

Apart from the monometallic NPs, particles could be built of different elements. Within this group, one can distinguish the core-shell type NPs. According to the naming convention, one material stays in the particle's core, and a different one, uniformly shields the core. Although both organic and inorganic materials can be used, in practical applications often inorganic nanoparticles are being applied because of their superior stability compared to organic compounds. The core-shell NPs can take many shapes, from a simple sphere-in-sphere and "nanomatryushka" to hexagons and single particle in an empty core (Radloff et al. 2004, Liu and Qiao et al. 2006).

Among others, silica is a very common shell material in a core-shell arrangement that provides many advantages. For example, its chemical inertness allows the occurrence of redox reactions through its protective layer without interfering with them, which is beneficial for catalysis or sensing purposes. However, it can also serve as a core material and alongside with metallic shell may be used to modulate the position of surface plasmon resonance band that can be registered by means of UV-vis spectroscopy, see Fig. 6 (Lee et al. 2006).

2.3 Dendrimers

Another interesting NPs examples are dendrimers whose name comes from Greek word “dendron” meaning “tree”. Those nanoparticles are recognized as nanosized macromolecules, with characteristic tree-like dendrons homogeneously cascading from its centre. The core of a dendrimer contains a small molecule or linear polymer that acts as an ovule for consecutive generations of dendrons bounded to the centre. Generally, dendrimers are synthesized using one of two approaches: divergent or convergent one (see Fig. 7).

Divergent method of dendrimer synthesis concerns the growth outwards from the dendrimer core, which reacts with monomer molecules forming further offshoots. Usage of this approach for production of more branched dendrimers requires even hundreds of steps. Therefore, as some statistical errors may to happen during the synthesis, finally non-perfect molecule could be obtained, e.g. the branches distribution is not homogenous. The question about the molecular shape of the dendrimer also arises, depending on the environmental conditions, as it is impossible to know if the dendrons are pointing outwards from their centre or if they are bending inside.

Convergent approach, however, relies on the synthesis of the outer molecular network first and subsequent reactions towards the core. This method allows higher degree of control over the synthesis because of significantly lower number of simultaneous reactions. The resulting dendrimer created by convergent approach can often be defect-free, although production of higher-generation dendrimers can be troublesome (Bosman et al. 1999, Abbasi et al. 2014).

Multitude of molecules can be used to create dendrimers, providing ways to tailor their properties with a specific task in mind. Because of the versatility of dendrimers, they are widely used in chemistry, pharmacy, bioengineering, and physics.

2.4 Fullerenes

Fullerenes are one of the many extensively studied allotropes of carbon. Although the most common and stable fullerene consists of 60 carbon atoms forming truncated icosahedron, their number can range from 20 up to a couple of thousands (see Fig. 8). The stability of C60 fullerene is associated with the strong covalent sp^2 bonds, where each carbon atom shares its valence electrons with exactly three neighbours through two single and one double bond. However, the position where the double carbon bonds appear, can be exchanged without structure destruction. Additionally, C60 fullerene is the smallest fullerene in which two pentagonal planes do not share an edge, as they can have a destabilizing effect on the structure (Manolopoulos et al. 1991).

In nature, fullerenes of varying sizes can be found in soot. It is also the source of their commercial production. One of the methods of synthesizing fullerenes is based on electric arc discharge between two graphite electrodes in the inert atmosphere. As the product, a fullerene-rich soot is produced and desirable fullerenes are extracted using appropriate organic solvents.

Applications for the fullerenes are wide. They can be used as MRI contrast agents, in drug delivery and for the inhibition of antibiotic-resistant pathogens proliferation (Tegos et al. 2005) . Particularly, in the medical application field, fullerenes are used as a photosensitizers for tumour removal process.

3 Nanowires

The nanowires (NWs) manifest promising properties as being the 1-D quantum systems nanoscopic in diameter and microscopic in length. Their unique properties

originate from phonon and electron size confinement in the direction perpendicular to the nanowire length. However, due to the different materials properties, observed effects of the size confinement differ enormously. For instance, metals exhibit a significant decrement of electrical conductivity when the nanowire diameter approaches the mean free path of electrons in the bulk material (Sofiah et al. 2018, Sannicolo et al. 2016), semimetals - a reduction of the U(I) dependency, semiconductors and insulators - an increment of the bandgap, and superconductors - an increment of the critical temperature.
The current section is divided into several parts, each describing another type of nanowire material. The first part is devoted to nanowires made of metals. Next, unique properties of nanowires made of oxides and semiconductors are discussed. In the fourth part, the variety of organic (including molecular) nanowires and their characteristics are shown. Finally, we conclude with the discussion of the superconducting nanowires.

3.1 Metallic nanowires

One of the commonly used transparent electrode materials is indium tin oxide (ITO). Despite its good optoelectronic properties, scientists try to find its substitute. Such an approach results from the fact that ITO is expected to become increasingly expensive and its brittleness is not compatible with the strong demands for flexible electronics (Sannicolo et al. 2016). One of the promising candidates is a film made of conducting nanowires so thin that their light transparency exceeds 90%. Herein, a few examples of metallic nanowires are presented.

Noble metals

Noble metal nanowires exhibit precious set of properties as high conductivity, environmental inertness, and flexibility (Sanicollo et al. 2016). Additionally, owing to the nanoscale diameter, metal nanowires are almost invisible for a human eye. Thus, the most perspective applications of noble metals are transparent, flexible electrodes, which should exhibit as high as possible light transparency. Yu et al. (2018) have shown that elongation of NWs length increases the strength of light back-scattering. As they showed, for the application as transparent electrodes of solar cells, silver NWs should be shorter than 20 μm. However, the decrement of NWs length may reduce the conductivity of the electrode due to the weakening junction between nanowires. The issue solution was proposed by Kim et al. (2018) who applied intense pulsed illumination for increasing silver nanowires temperature, and in a consequence, for welding of individual Ag NWs without damaging the PET substrate.
Noble metal nanomaterials are also known to be efficient catalysts for electrochemical reactions in the field of energy conversion and for chemical reactions in the chemical industry. However, due to their high price and decreasing resources, the elaboration of new highly effective modified noble metal based materials including noble-transition metal alloys and transition metal wires covered by the noble metal is required (Greely et al. 2009).
For instance, Dai et al. (2016) obtained $PtCu_3$ (Koenigsmann et al. 2013) synthesized ruthenium nanowires as thin as 44 nm utilizing a template-based method under ambient conditions. However in 2016, Zhao et al. (2014) obtained even thinner Ru and Ru/Pt nanowires (with a Ru/Pt relation from 50:50 to 73:27) of an extremely low diameter of 1.5 nm via an aqueous approach. Using the element mapping analysis, the authors revealed that the Ru and Pt were uniformly distributed in the nanowire networks forming a solid-solution alloy. The obtained material was

tested for the electro-catalytic activity towards the methanol oxidation. Results have shown that the RuPt nanowires displayed promising composition dependent properties.

Non-noble metallic nanowires

Due to the high price of noble metals, transition metal NWs are examined as the cheaper substitution. Kim et al. (2016) demonstrated a synthesis route to fabricate 60 μm-long nickel nanowires, which displayed to be a good candidate for use in transparent conducting electrodes. A transparent electrode made of Ni NWs showed transparency as high as an ITO electrode for the same effective resistivity. The authors even suggest that obtained electrodes are more suitable as a bottom OLED layer than ITO or Ag nanowires.

Another material considered as a promising candidate for transparent conducting electrodes is copper as nanowires. Until now, Cu NWs with a diameter of 60-80 nm and length over 50 μm were successfully synthesized by a modified self-catalytic method (Zhai et al. 2018). Although their transparency is not as high as that of the noble metal, it is still relevant to use in semi-transparent solar cells.

Another interesting group of materials is semimetals characterised by a narrow bandgap. Bismuth is a semimetal frequently serving as a typical model for investigations on semimetals. Due to its band structure, small electron concentration and electron scattering, the effective electron mass is very small and the Fermi wavelength (electron wavelength at Fermi level) equals 40 nm. As a consequence, free electron path length becomes extremely large and reaches even up to 1 mm at T = 4.2 K. Additionally, in semimetal nanowires, as in other metals, decreasing the size causes other effects like a cut off the phonon spectra, and the drop of the thermal conductance.

3.2 Oxide nanowires

As well as metallic, metal oxides attract great attention among nanowires. They are characterized by lower conductivity but exhibit other useful properties like tunable bandgap, wavelength dependent transparency and catalytic properties. For instance, ZnO NWs of ~5 μm in length and ~120 nm in diameter on a p-type GaN (Fig. 9) find an application as a nanowire nanolasers (Huang et al. 2017). The wires play a double role, both as an optical resonator when the wire length is divisible on the integer number of half-waves and an active medium. A spontaneous emission arises when current power overcomes a lasing barrier, which under irradiation of the laser beam of 355 nm wavelength is 180 mW/cm^2. Such a ZnO nanowire assisted laser possesses a relatively small lasing threshold owing to bulk ZnO parameters and operates in a single-mode regime due to the low length of wires.

Another unique property of NWs made of semiconductors and insulators is ultra-low thermal conductivity. Because of the high surface-to-volume ratio of nanowire, the surface phonons modes start to play an important role in phonon scattering. Their interaction with the longitudinal and transverse phonons as the boundary scattering within the nanostructures, leads to a decrease in the phonon lifetime. Thus, the phonon transports and the thermal properties of the nanowires significantly decrease compared to that of the bulk material.

Spinel nanowires have found an application in the field of the electrochemistry cells and catalysts. Thanks to a high specific surface and a high defect concentration, spinel nanowires are considered being an effective substitute for platinum catalysts. For example, Liu et al. (2018) have found that hydrothermally synthesized $NiCo_2O_4$

nanowires after transformation to the $NiCoO_2$ became a very active catalyst due to a high concentration of oxygen vacancies.

3.3 Non-oxide semiconducting nanowires

Bendable electronics have attracted widespread attention because of their potential application in many smart electronic devices and flexible displays. Therefore, high attention is paid to the research on bendable electronic elements, like diodes, transistors, capacitors, etc. Because of their elasticity, 1-D and 2-D nanostructures are intensively studied. One of the study achievements are bendable NAND logic gates with silicon nanowire channels capable of operating with a supply voltage as low as 0.8 V (Yun et al. 2016) . The gate was based on a Si nanowires with a 40 nm diameter prepared via low-pressure chemical vapour deposition, ion implantation doping, and finally deposition onto a plastic substrate.

III–V semiconductors are considered as a beneficial material for optoelectronic devices such as multi-junction solar cells due to their broadly tunable bandgaps. Thus, III–V nanowires are even more interesting, since they add new benefits for nanophotonics devices like increased optical absorption compared with the bulk material caused by light-trapping effects. Moreover, NWs are expected to reduce the materials consumption of these relatively expensive semiconductor materials in the future. For example, a comparison of planar and nanophotonic geometries of InPb (cui et al. 2016) NWs with the same material quality, indicates that the external radiative efficiency of the nanostructured layer is 14-times enhanced compared to those found for the planar coating. The higher efficiency arises from the enhanced out-coupling of photons promoting radiative recombination and the lower active material volume, which reduces bulk recombination.

Another common approach used for the preparation of III-V semiconductors is the metal-seeded vapour-liquid-solid (VLS) technique. Berg et al. (2017) synthesized InGaP nanowires as low as 30 nm in diameter (see Fig. 10). They have shown that the uniform growth was achieved in a temperature range of 675 - 750°C, while increasing of the synthesis temperature leads to the increasing of a nanowire deformation degree and decreasing of the nanowires length simultaneously.

The regularly dispersed nanowires can also be obtained by the self-assembled formation processes. One example is the self-assembled formation of GaN nanostructures obtained by the plasma-assisted molecular beam epitaxy on the TiN substrate van Treck et al. 2018). Using this approach, van Treck et al. (2018) were able to obtain nanowires of the diameter less than 50 nm and of a homogeneous length of more than 1 μm. It is worth noting that the separation distance between nanowires is caused by the diffusion-induced repulsion of neighbouring NWs, without using a templated substrate.

It is known that the composition defects could substantially alter the properties of semiconductors. Therefore, incorporation of foreign non-equilibrium atoms in the host semiconductor lattice may be used for new or added functionalities in the existing semiconductor system (Yin et al. 2008) , namely strain engineering, controlled defect formation, band structure modulation, etc. For example, a non-equilibrium incorporation of Sn in Ge induces the small energy band variation, which makes them a direct bandgap semiconductor (Yin et al. 2008) . The non-equilibrium Sn-Ge alloy was obtained by a “solute trapping” process. At the certain solidification rate, during the vapour-liquid deposition growth of nanowire (Fig. 11) a local chemical equilibrium at the liquid – solid interface cannot be settled due to a large interface velocity. Therefore, Sn atoms can be trapped on the unfavourable

energy sites of the nanowire crystal lattice leading to the formation of metastable solids at the nanowire growth front.
Some optical properties of III-V semiconductor nanowires may also be improved by their surface treatment. For example, a deposition of parylene-C, a highly resistive transparent polymer, onto the GaAs followed by an annealing, decreases the system reflectivity below 1%, what strongly improves its absorbance and photoluminescence intensity (Haggren et al. 2017).

3.4 Organic nanowires

Despite inorganic materials being much more popular when considering a quantity of scientific reports, such elongated structures are also formed by organic compounds. Organic nanowires have inherent advantages related to low-cost and low-temperature processing, since in many cases, further thermal treatment is not required.
The high success of carbon nanotubes led to the initiation of research devoted to other organic elongated forms of nanomaterials. For example, Lentz et al. (2011) developed a method which allows to obtain amorphous carbon nanowires. The semiconducting nanowires with an average diameter of 150 nm were synthesized by a pyrolysis of polymerized polyfurfuryl alcohol inside the pores of an anodized alumina template. The thinner NWs were obtained from the paralyzed bacterial cellulose. Nitrogen- and phosphorous-doped 50 nm thick carbon nanowires obtained by Hu et al. (2016) showed promising properties for supercapacitors like capacitance density of 258 F/g at a current density of 1 A/g and exhibited an excellent cycling stability over 30,000 cycles.
Pyrolysis, as a synthesis method of organic NWs, limits control of the morphology, especially, the fabrication of molecular nanowires with a diameter below 100 nm is very hard to control. Therefore, the application of organic nanowires in optoelectronic devices is a big challenge. However, in the work of Tan et al. (2016) the first demonstration of the highly ordered organic single-crystalline nanowires can be found. The nanowires are fully composed of self-assembled small organic molecules, which next are successfully used as a Fabry-Pérot optical resonance cavity for 720 nm NIR nanolasers.
In most cases, nanowires are obtained via chemical, electrochemical or physical methods. However, in recent years, a new branch of nanowires fabrication methods has been elaborated. Among them, biological synthesis is potentially attractive because it allows the obtaining of nanowires from a fully renewable resources. Moreover, the final product may be obtained without the need for toxic solvents or harsh chemical processes (Tan et al. 2016). An attention is paid to *Geobacter sulfurreducens* (Reguera et al. 2005) as one of the electrically conductive pili, due to its high aspect ratio (3 nm × 15 μm). Tan et al. (2016) have shown that manipulation within the genotype of *G. sulfurreducens* allows to produce conductive nanowires of a diameter below 2 nm and over 3 μm in length. It is worth noting that the authors measured the final conductivity of the nanowires only one order of magnitude lower than observed for carbon nanotubes (Tans et al. 1997).

3.5 Superconducting nanowires

The last materials discussed in the current subsection are superconductors. These specific group exhibits its unique properties below the critical temperature, therefore a discussion about its high-temperature characteristic is neglected.
Similarly to other properties, critical temperature of superconductivity is size-dependent as well (Mooij et al. 2015). For example, transport measurements of

individual cylindrical single-crystal Bi NWs, 20 and 32 nm in diameter, have shown that, in contrast to non-superconducting bulk or Bi nanoribbons, cylindrical Bi nanostructures exhibit superconductivity at the temperature as high as 1.3 K (Tian et al. 2015).
One of the most interesting phenomenon observed in the superconducting nanowires is a manifestation of Majorana fermions (Mourik et al. 2015). They are specific particles identical to their own antiparticle, hypothesized by Ettore Majorana in 1937. In 2008 Fu and Kane (Fu and Kane 2008) have shown that these specific particles may be observed on the junction of superconductor and metal, what was finally proven a few years later.

4 Nanowalls

The nanowalls, often named nanosheets, manifest promising properties being the 2-D quantum systems nanoscopic in thickness but microscopic in length and width. A great interest in two-dimensional material arose after the exploration of graphene. Nowadays, other classes of 2-D nanomaterials are known, like single- or few-layered transition metal dichalcogenides, metal oxides, layered double hydroxides, hexagonal boron nitride (h-BN), graphitic carbon nitride (g-C_3N_4), metal carbides and nitrides, and monoelemental compounds (Chia and Pumera, 2018) . Their specific area is theoretically not as large as nanowires. However, this feature, sometimes regarded as a disadvantage, is diminished by much more facile synthesis compared to 1-D structures (Zhou et al. 2013). The outstanding properties of selected 2-D nanomaterials are described in four sections, each devoted to one family of nanowalls/nanosheets: semiconductors, oxides, carbon-based materials and composites.

4.1 Semiconducting nanowalls

2-D materials are found to be chemically inert, have high mechanical strength and thermal conductivity in a parallel to the plane direction, while their parameters may urgently differ in the perpendicular direction. The most well-known 2-D and widely applied nanomaterial is graphene. However, other compounds, including hexagonal boron nitride (h-BN) can be obtained as a single- or few-walled nanomaterial. Besides typical for 2-D materials properties, its multi-layered structure exhibits deep UV luminescence, and, what is more interesting, vertically aligned nanowalls of h-BN were found to be cytotoxic against *E. Coli* (Merenkov et al. 2019*,* Zhang and Feng et al. 2017). Although several methods of h-BN preparation have been elaborated, the most successful way to obtain nanowalls is a CVD method (Merenkov et al. 2019). The growth mechanism of the less than 15 nm thick nanowalls is shown in Fig. 12. At the beginning, the interfacial layer is formed. Then the nucleation of several plane nanocrystallites takes place, which grows in the plane until neighbouring layers contact each other. Finally, one of the layers turns upward and the vertical growth appears.
It is known that the effectiveness of catalysts depends on their specific surface area, therefore, 2-D semiconducting nanomaterials are expected to be highly effective. For example, CuS nanowalls were used for the thermal decomposition of ammonium perchlorate (Yao et al. 2017). The presence of CuS nanowalls decreases the temperature of the ammonium perchlorate decomposition for over 150°C, from 312°C to 145°C. It is worth to note, that the synthesis of CuS nanowalls was performed not on the solid substrate, but at the liquid-liquid interface of chloroform and water, which leads to the formation of a 2 μm layer composed of weakly joined CuS nanowalls.

The bandgap of nanomaterials undergoes a widening with decreasing size due to quantum confinement effects. This statement was a background for the study performed by Ichikawa et al. (2017) on the 2-D Si quantum well structure. Using anisotropic wet etching, the authors were able to fabricate high-quality Si nanowalls as thin as 3 nm with vertical flat sidewalls at the Si/SiO_2 interface. However, they were unable to record the variation of the optical bandgap because of the light dispersion on the regular nanowalls structure.

4.2 Oxide nanowalls

Nanowalls were also formed by oxide materials which find applications as effective gas sensors, highly capacitive electrodes, optical modulators, an active transistor channels material, and others. For example, ZnO is a direct-bandgap n-type semiconductor material (E_g = 3.37 eV) which may find application as a hazardous gas sensor. However, its functionality is limited by high working temperature, low electrical conductivity, and poor thermal stability. Kim and Shim et al. (2017) tested Nb doping of ZnO nanowalls, what increases the specific surface area of the sensor in comparison to that of pristine ZnO nanowall by ca. 10%, improves its conductivity and decreases possible operating temperature.

The interconnected nanowall structure can offer excellent charge transfer path and provide large contact specific areas of electrolyte/electrode interfaces. Therefore, highly capacitive electrodes made of transition metal oxides nanowalls, like CoO, NiO or MnO_2, are considered being good candidates for electrodes in supercapacitors. Tang et al. (2019) examined properties of the CoO porous nanowall structure obtained by a combination of solvothermal growing and annealing. It was shown that the morphology of CoO nanowalls can be tuned by adjusting the annealing temperature. In particular, nano-sized pores below 50 nm are formed on CoO nanowalls during thermal treatment. The unique porous nanowall structure leads to a large specific surface area (65 m^2g^{-1}), which increases the electrolyte/electrode interface. Following that, enhanced electrochemical performance of CoO was obtained.

Electrochromism is another interesting property of transition metal oxides. Zhang and Zheng et al. (2017) synthesized Co_3O_4 nanowalls via hydrothermal method. The product exhibited highly porous nature and large surface area. Due to that, fast and large optical modulations are realized in the Co_3O_4 nanowalls.

Transition metal oxide nanowalls are considered finding applications in nanoelectronic devices. However, due to strong electrons correlation in metal oxides, a rich variety of electronic phases with unique properties including superconductivity, colossal magnetoresistance or metal-insulator transition, is observed. Therefore, control of that electric phases, especially in a field-effect transistor seems to be very promising. Hattori et al. (2018) fabricated an electric double layer transistor with a $(La,Pr,Ca)MnO_3$ channel and investigated the gating effect. The nanowall was fabricated by combining UV-nanoimprint lithography, pulsed laser deposition, etching and annealing processes. The reported transistor is the first based on the control of the insulator-metal transition.

4.3 Carbon-based nanowalls

A distinctive family of nanomaterials is a transition metal oxide nanowalls deposited onto the carbon nanowalls. Due to the high conductivity of carbon-based materials and high electrical capacity of transition metal structures, they found an application as electrodes in the Li-ion batteries or supercapacitors (Dai et al. 2017) . Zhu et al. (Zhu et al. 2011) reported on ultrathin Co oxides nanowall arrays deposited on

reduced graphene oxide (rGO) sheets. In that nanohybrid system, the Co oxides exhibited a porous structure and the grain size of the Co oxide was tailored by varying the annealing temperature.
Carbon nanowalls attract attention also due to their specific electrical properties, including a resistive switching phenomenon. Russo et al. (2017) have reported for the first time the resistive switching behaviour of a device made of carbon nanowalls deposited on a fluorine-doped tin oxide substrate. The carbon nanowalls were synthesized by electrophoretic deposition from the solution of polyynes. The obtained memory resistive switching device showed an operation voltage of 2 V and long retention time (over 10^4 s). Those parameters suggest that carbon nanowalls may be used in the future as a basis of commercially available memory devices.

5 Nanopores

Ordered self-standing porous materials offer a wide range of possible applications, since they can be used as a ready product for certain processes, e.g. drug transport, catalysis, investigations of adsorption or separation processes and a substrate for further synthesis of materials that morphology can project the substrate shape. Following that, nanopores can act as a template for nanotubes or nanowires production as well as a patterning mask. Furthermore, elaboration of novel manufacturing techniques that allow to control geometric parameters of internal pore structure can develop other materials based on the template assisted synthesis.

5.1 Porous anodic aluminium oxides

Aluminium, as typical oxidizing materials, exposed to air spontaneously forms a thin barrier oxide layer. The very thin barrier oxide film, called passive layer can also be obtained via electrochemical oxidation in much more controlled way. Anodizing in the electrolytes of pH = 5 - 7, such as borate, oxalate or citrate with the respect to the other conditions forms compact passive layer on aluminium plate. However, usage of acidic solutions such as selenic, sulfuric or oxalic partially dissolves aluminium oxide whereas simultaneous electrochemical oxidization under the optimized conditions enables formation of porous anodic aluminium oxide (AAO) layer (Lee and Park 2008).

Self-ordered porous AAO with a uniform pore size and distance can be achieved via two-step anodization, so-called mild anodization (MA). The first anodization typically takes over 24 h. In the next step photochemical etching is carried out that concerns oxide layer removal by the immersion of as anodized alumina in sulfuric acid and chromium oxide mixture at the elevated temperature. The process results in the wells-like morphology formation onto the remaining aluminium substrate. Owing to such procedure, nanopores grown during the second anodization are uniform and parallel to each other. Moreover, pores diameter, distance between them and thickness of barrier layer can be controlled by an applied voltage and electrolyte composition. MA allows to reach the growth rate within 2 – 10 μm/h range. On the contrary, hard anodization (HA) performed at the voltage exceeding breakdown potential allows for much faster growth rates up to 50 – 100 μm/h. Such a high voltage generates very high current flow, 1 or 2 orders of magnitude higher comparing to MA. As a consequence, large amount of heat causes spatial damages in morphology. Since the geometric parameters of the material are out of control and the morphology destructions are present, HA has not found applications in nanotechnology (Lee et al. 2014).

Sequential combination of MA and HA by applying alternately low (mild anodization voltage) and high (hard anodization voltage) potentials allowed to obtain modulated internal pore diameters within AAO. This concept, so called pulsed anodization (PA) is regarded as a beginning for the further structural modifications in AAOs by cyclic anodization (CA). The technique requires applying oscillating current signals with different parameters such as period or amplitude to electrodes. It allows formation of different pore geometry (Lee et al. 2008). According to PA approach, tailor-made AAO pore structure can be prepared as shown in Fig. 13 a whereas polymer nanopillars obtained inside such template is shown in Fig. 13 b.

Apart from anodization of aluminum foil itself, ordered structures can be obtained by anodization of sputtered Al films on different substrates such as insulators, semiconductors, non-valve metals, valve metals or transparent indium thin oxide. The most widely investigated was anodization of Al thin film deposited onto the Si substrate resulting in interfacial voids formation at the bottom of pores (see Fig. 13 c). This phenomenon is related to the stress accumulation and its minimizing. It is worth noting that for longer anodization times SiO_2 nanodots are formed underneath the voids due to the Si oxidation by electrolyte migrating through the small hollow spheres located below elongated pores.

Long-range arrangement with a high degree of uniformity that is required for the most applications can be achieved by anodizing nanoimprinted pattern on aluminum substrate. The shape and position of that pattern define very precisely further nanopore arrangement. However, still obtaining almost ideally ordered porous AAO depends on appropriate adjustment of the anodization parameters. According to that procedure, AAO diamond pattern template was fabricated by Seo et al. (2007), see Fig. 13 d.

5.2 Porous anodic titanium oxide

As was already discussed, anodization of aluminum enables AAO formation. Whereas, anodization of other valve transition metal, namely titanium may provide two different morphologies: nanotubes or nanopores depending on the anodization parameters such as: anodization time, temperature, applied voltage or fluoride ions concentration (see Fig. 14 a) (Sulka et al. 2010). Pore formation mechanism is directly related to the chemical etching of titanium during anodization. Suitably low titanium etching rate causes growth of TiO_2 on the sides of the nanotubes entrances (Yan and Zhou 2011). As the consequence, pores form interconnected nanotube architecture. Schematic diagram depicting pore and tube growth is given in Fig. 14 b.

Titania structures i.e. nanotubes and nanopores obtained via anodization are in the amorphous phase. Therefore, calcination in a furnace is usually performed to ensure the crystalline phase. It is worth mentioning that the whole process covering the heating up of samples and their cooling down to room temperature can take over 10 h. Since there is a competition between pore and tube formation during anodization and as-anodized titania requires phase conversion, the number of reports on TiO_2 nanopores synthesized via electrochemical oxidation is not that much as for AAO.

6 Nanotubes

As has been already underlined, nanostructures with an increasing specific-surface area are of high importance for catalysis, sensing, or light harvesting. Nanotubes (NTs) because of hollow-like structure and the high aspect ratio (length-to-diameter) have an available surface on the inner and outer wall that makes surface area higher

comparing to nanorod where only outer sphere could form interface. Moreover, the 1-D tubular geometry improves electron transport for longer distances and facilitates light absorption (Samadipakchin et al. 2017). Due to unique properties, different NTs have found various applications, especially in solar cells and sensors. The most commonly known nanotubes are those made of carbon, TiO_2, and ZnO.

Carbon nanotubes (CNTs) have high tensile strength and Young's module at relatively low density of this material (Paradise and Goswami 2007). They also exhibit extraordinary thermal conductivity (Han and Fina 2011) and unique anisotropic electrical properties. Extremely high conductivity values of CNTs (such as 20,000 S/cm) can be achieved. However, in this case, many purification steps are required for this purpose (Lekawa-Raus et al. 2014). Therefore, it is important to regard all the pre- and post-processing treatments while considering the reported conductivity values of CNTs by different authors. Due to the unique properties they have found many applications for: medicine including drug delivery or tissue engineering, biosensors (Raphey et al. 2019) , gas sensing (Han et al. 2019) , carbon-reinforced matrix composites (Hynes et al. 2019) and others.

Titania nanotubes are as other titania geometric forms n-type semiconducting functional material with a large bandgap of 3.2 and 3.0 eV for anatase and rutile polymorphic forms, respectively. Due to that, light absorption of TiO_2 is limited only to the UV part of the solar spectrum. However, it can be enhanced by doping with metals, nonmetals or semiconductors (Chen et al. 2013) . Taking into account the facile control of geometric parameters of NTs during anodization, excellent photocorrosion resistance of TiO_2NTs and their appropriate band edge positions they have found applications in dye-sensitized solar cells (DSSC), pollutants degradation, water splitting, membranes, sensors and others (Lee et al. 2014).

Apart from TiO_2, ZnO is also regarded as a low cost, non-toxic, n-type semiconductor but its direct bandgap of about 3.37 eV is even larger than for titania. Moreover, it has higher electronic mobility and synthesis of different morphologies such as nanowires, nanosheets or hollow spheres is possible in comparison to TiO_2. Since ZnO has suitable band structure for both water reduction and oxidation, ZnO NTs are investigated as a photoanode material for hydrogen production via photoelectrochemical water splitting process Long et al. 2019), in solar cells (Shen et al. 2019) or for gas sensing (Choi and Chang 2018) . As it can be seen ZnO NTs and TiO_2 NTs have similar properties and applications. However, the huge advantages of the electrochemical anodization over ZnO NTs manufacturing methods make this material only to be considered as a replacement for TiO_2 NTs.

6.1 Carbon nanotubes

CNTs were synthesized for the very first time by Sumio Iijima in 1991 (Iijima 1991). They can be considered a "rolled" graphene sheets while graphene is a single layer of carbon atoms arranged in a hexagonal network. Depending on the number of rolled layers CNTs can be single- (SWCNTs), double- (DWCNTs), or multi-walled (MWCNTs). Figure 15 shows SW- and MWCNTs structures whereas their comparison is shown in Table 5. Taking into account the direction of how graphene sheet is rolled different CNTs arrangements can be formed such as: zig-zag, chiral or armchair.

Among SWCNTs, one can find three various structures (see Fig. 16) obtained by rolling graphene sheet in different directions in an accordance with the values of a chiral a_1 and a_2 vector pair. Knowing that the spatial arrangement impacts the material properties, a diversity of carbon tubular forms offers a wide range of applications.

In the literature there are three main approaches based on carbon precursor decomposition allowing fabrication of CNTs: arc discharge, laser ablation and chemical vapour deposition. Classification of CNTs manufacturing methods with more detailed distinction of CVD approach is shown in Fig. 17.
Concerning arc discharge, the method involves electrical breakdown by DC current of a gas to generate plasma. It results in temperature increase at the graphite anode where the carbon precursor is evaporated and deposited onto the graphite cathode. The process takes place in a vacuum chamber with a controlled supply of inert gas, argon, or helium. Both SWCNTs and MWCNTs can be produced via an arc discharge approach. However, in the case of SWCNTs anode filled with catalysts such as Fe, Co, Ni is essential. Catalyst facilitates the decomposition of carbon from the precursor at a lower temperature. Nevertheless, it makes the production process more expensive (Kumar et al. 2017, Zulhairum et al. 2019, Mohamed 2019).
The laser ablation technique is a quite similar approach to arc discharge. It requires high energy laser radiation to ablate graphite from the target under the inert gas atmosphere which is further deposited on the substrate. As was in the case of the arc discharge, SWCNTs and MWCNTs can be produced. However, this method allows to fabricate smaller quantities of CNTs compared to the arc discharge (Kumar et al. 2017, Zulhairum et al. 2019, Mohamed 2019).
Nowadays, the most widely used manufacturing technique for different CNTs is CVD. This method involves the pyrolysis of carbon precursors such as acetylene, ethylene, propylene, methane, polymers, or carbon monoxide. Vapors generated in this process are transported using the inert gas to the chamber containing the catalyst. It is worth mentioning that catalysts act here as nucleation sites for CNTs growth. CVD enables large-scale production due to the high yield rate and relatively simple equipment compared to machines needed for arc discharge and laser ablation methods. It also enables control of the growth process and ensures good alignment. The diameter of the NTs can be adjusted simply by the temperature knowing that the CNT diameter is directly proportional to the applied temperature. Temperature also determines whether SW- or MWCNTs are formed. Higher temperature (ca. 900°C) favors SWCNTs formation, whereas lower temperature (630°C) supports the synthesis of MWCNTs (Kumar et al. 2017).

6.2 From 1st to 4th generation of TiO_2 NTs

Since the first reports on self-ordered TiO_2 NTs obtained via electrochemical anodization have been released, this technique has attracted more and more attention due to its relative simplicity and ability to control the geometric parameters of the NTs. Moreover, it can be easily scaled up and growth of TiO_2 on large Ti substrates is possible. In the literature evolution of TiO_2 NTs has been classified into the four generations due to the various types of electrolytes used in the process. Brief summary of TiO_2 NTs evolution is shown in Table 6.
Initially, the anodization was performed in the aqueous inorganic HF-containing electrolytes which represents the 1st generation of TiO_2 NTs. Since acidic solutions are an aggressive media accelerating chemical dissolution of the barrier layer, the length of 1st generation NTs reaches only a maximum of ca. 500 nm. Moreover, NTs exhibit a rippled structure due to the presence of fluoride ions originating from HF dissolved in a water bath. The 2nd generation is based on the usage of buffered solutions with the addition of fluoride ions in the form of an inorganic salt such as Na_2SO_4/NaF or $(NH_4)_2SO_4$/NH_4F. Reduction of acidity by excluding HF from the solution allowed to obtain NTs even up to 5 μm length. However, the morphology of 2nd gen. NTs is still rippled due to aqueous solutions. Irregularities in the 1st and

2nd generations of the NTs might be related to oxygen bubbling in water solutions, which occurs on the anode surface during anodization. The presence of water is a key factor in ribs formation. Contrary to previous 1st and 2nd approaches, 3rd generation of TiO_2 NTs is based on organic electrolytes with the addition of F^- ions and low water content. In this type, both smooth or rippled structures can be formed depending on the water content. Below 0.5 wt.% of the water threshold the NTs are smooth and no ripples are formed. The 3rd generation of TiO_2 NTs allows to manufacturing up to 1000 μm-long NTs. Morphology can be controlled by potential, water content and time in ethylene glycol solution. It is worth noting that depending on organic solvent type it is possible to space out NTs. Ozkan et al. (2018) obtained spaced (SP) NTs in diethylene glycol and dimethyl sulfoxide solutions. Such a change in the morphology affects significantly optical, electrochemical and photoelectrochemical properties of the NTs. Close-packed (CP) NTs provide higher surface area and may exhibit higher electrochemical activity. However, in the case of photoelectrochemical performance, SP NTs are more efficient due to the unique morphology in which spaces between NTs act as traps for incident light. Moreover, SP NTs show faster charge transport compared to CP ones. Therefore, due to the enhanced light harvesting by free-standing NTs they might be a promising material for photoelectrochemical water splitting or solar panels.

Concerning the 4th generation of TiO_2 NTs, the classification is not completely clear. In the literature some researchers classify NTs obtained in fluoride-free electrolytes to the 4th generation (Huang et al. 2013, Wang et al. 2017) , . This unique approach is called rapid breakdown anodization (RBA) and it is performed in perchloric acid ($HClO_4$). RBA allows to obtain several dozen micrometers long NTs within few minutes. However, RBA provides irregularities in the NTs morphology and high aspect ratio is achieved only within bundles (Hahm et al. 2007) . Therefore, RBA is rather used to manufacture TiO_2 NTs powders (Ali and Hannula 2017, Arunchandran et al. 2013). On the other hand, there are reports classifying 4th generation of NTs to fluoride-containing organic electrolytes (similar to 3rd generation) but with a strict consideration of anodization parameters such as fluoride concentration, anodizing potential and time (Regonini et al. 2013) . In this case highly ordered hexagonally close-packed arrays can be achieved by a multi-step approach, where anodization steps and etching of as-formed titania are repeated.

Summarizing, electrochemical anodization is a relatively simple technique that allows to synthesize a wide range of TiO_2 NTs structures with various morphologies. The development of the four TiO_2 NTs generations has allowed to manufacture short, long, ribbed, smooth, spaced or close-packed NTs. Such a facile control over the NTs morphology allows to elaborate almost ideal geometry for particular applications. Due to that, TiO_2 NTs have been one of the most studied materials in the last decade.

6.3 ZnO nanotubes

As has been already mentioned, ZnO NTs do not have one leading manufacturing method as in the case of TiO_2 NTs. There are several approaches for ZnO NTs formation that can be divided into three groups: physical, chemical (hydrothermal) and electrochemical methods. A brief summary of ZnO NTs manufacturing methods with a SEM micrographs of morphology is shown schematically in a diagram given in Fig. 18.

Physical methods are based on deposition of the ZnO from its precursor onto the template using a thin layer coating techniques such as atomic layer deposition (ALD), magnetron sputtering (MS) or CVD. Within the first approach core-shell

structures are manufactured and the following template removal ZnO NTs remain. Zhang et al. (2015) synthesized ZnO NTs via ALD on AAO templates. After the material deposition, AAO template was removed by etching in a 0.1 mol/L NaOH water solution (Zhang et al. 2015). Choi and Chang (2018) obtained porous and nonporous ZnO NTs by deposition of Zn via radio frequency magnetron sputtering on the polyvinyl acetate (PVA) core nanowires obtained by the electrospinning method. The PVA nanowire core was subsequently removed by calcination in the furnace at 550°C for an hour at the reduced pressure[Błąd! Nie zdefiniowano zakładki.]. Basing on another approach, Zhang et al. (2019) synthesized Ag-ZnO cored NTs on Si wafers decorated with Au particles via CVD inside a quartz tube furnace. As source materials, they used the mixtures of Ag and ZnO powders. Once the temperature in the furnace reached 800°C, Ag vaporizes and is deposited onto the Au particles. In this method, Ag forms a wired structure on the Au particles. Next, the temperature in the furnace was set to 1300°C. Zn vaporized and following deposition on Ag-core led to Ag-ZnO NTs structures.

ZnO NTs growth can be also supported by the electrochemical deposition. Long et al. (2019) proposed a simple three-step strategy to obtain ZnO/$ZnFe_2O_4$ NTs onto FTO glass. In this procedure, ZnO NTs are achieved in the following steps:

(1) Synthesis of ZnO nanorods through electrochemical deposition in $Zn(NO_3)_2$-containing electrolyte at the elevated temperature for 1.5 h,
(2) Etching of the inner part of ZnO nanorods by soaking ZnO nanorods in 0.18 M KOH warm solution for an hour, washing with ultrapure water, drying
(3) Annealing at 400°C for 30 min.

The hydrothermal method represents a different approach in which tubular structure is achieved by chemical reactions performed at the elevated temperature. Here, concentration of chemical compounds, temperature, pH and synthesis duration play an important role on nanotubes formation and their morphology. Samadipakchin et al. (2017) elaborated solution-based method in which ZnO formation occurred in the series of reactions of $Zn(NO_3)_2$ and NH_3. They used $Zn(NO_3)_2 \times 6H_2O$ and polyethylene glycol (PEG) as a precursor and liquid environment, respectively. Then, NH_3 was gradually added to the mixture to set the pH solution to 10. The reaction was carried out at elevated temperature. After the reaction was finished, the residue reactants were cleaned by distilled water and ethanol. The product was finally dried in an oven at 60°C under air atmosphere. The morphology of ZnO NTs obtained via hydrothermal method is a bush-like and exhibits a low degree of ordering.

7 Mimetic nanomaterials

The word mimetic comes from Greek mīmēsis, which means “to imitate”, therefore mimetic materials ought to imitate nature in some way, shape or form. In nanotechnology, the term is used when material, molecule or particle looks like an object or performs a function similar to one present in natural world.

Materials visually mimicking nature are usually not the goal of the research itself. Scientists tend to pursue improved properties rather than visual appeal of new structures, nonetheless, developed nanostructures sometimes yield shapes that look oddly familiar. Thanks to their unique combination of morphology and properties, these kinds of structures have been gathering interest in both the press and scientists throughout the years.

Herein we describe selected examples of mimetic nanomaterials, their synthesis, properties and possible applications.

7.1 Nanotrees

Indium tin oxide is a transparent, conductive material, commonly used in touchscreens, light-emitting and photovoltaic devices. Chemical vapour deposition method, often used for production of ITO coatings, allows only the formation of a thin layer on the surface. However, it is widely accepted, that in order to achieve improved photovoltaic devices, high surface area is necessary. To reach this goal, nanotrees were formed using modified CVD method, called vapour-liquid-solid (VLS) combined with glancing angle physical vapour deposition (GLAD). While VLS allows for rapid adsorption of deposited material, the angle of deposition can be directed using GLAD. The combination of both techniques allows for growth of tree-like branching nanostructures. Nanotrees produced with VLD-GLAD technique can be successfully applied in photovoltaic devices. Developed surface area improves photoactivity by an increasing number of excitons generated within the material, compared to devices based on flat ITO. Additionally, they can be used as a protein or gas sensing devices or UV light generators (Beaudry et al. 2012). On the contrary to much demanding CVD, simple hydrothermal oxidation has been proposed for tree-like ZnO arrays formation (Zhao et al. 2010) . Branched nanotrees shown in Fig. 19 were grown onto the cheap Zn supports and detailed TEM analysis confirmed wurtzite crystals growing mainly in [0001] direction. Usage ethylenediamine as a co-solvent allows for the morphology control and complexing of ZnO unique structures. What is of high importance, the proposed method is one-step, low-cost and environmentally benign to produce large scale and densely packed arrays exhibiting pure phase whereas their morphology could be easily tuned. Owing to the applied synthesis conditions, at a relatively low temperature much more complex nano- /microstructures might be obtained (see Fig. 20). The formation of developed ZnO structures is reached by modification of three main parts of nanotree: top, branches and stem. For example, the stem structure can be controlled with single, coalescent and splitting growth behaviour. Such expanded nanostructures can find application in mechanical, chemical, optical and electronic fields.

7.2 Nanoflowers

Nanoflowers are the most diverse family of mimetic nanoparticles, owing it to the multitude of easy ways to synthesize them and many possible applications of this kind of materials. They are usually synthesized by reducing noble metal salts and their entrapment with a surfactant in order to prevent their agglomeration and degradation.

Adding dopamine hydrochloride to chloroauric acid results in the rapid precipitation of gold nanoparticles. In this process dopamine acts both as reductant and shaping agent, so its amount determines shape and size of the nanoflowers (Fig. 21). These structures are particularly efficient as a platform for surface-enhanced Raman spectroscopy (SERS) and thanks to their low c-toxicity they can be used in cellular research and biomedical applications in particular (Hu et al. 2014).

Another way to create flowery, organic nanogarden is to incorporate rolling-circle replication (RCR) method to create DNA-based nanoflowers, see Fig. 22 (Hu et al. 2014) . RCR, as an isothermal enzymatic reaction, can rapidly synthesize multiple DNA or RNA molecules which are used as a building blocks for the flowers synthesis through liquid crystallization.

Flowers-like nanomaterials obtained in such way exhibit exceptional stability in biological and denaturing conditions, therefore could be recognized as promising

candidates for research in biotechnology. Additionally, adsorption of molecular dyes onto the surface of nanoflowers, allows them to be used as a traceable fluorescent drug carriers.
There are also reported examples of organic-inorganic flower structures (see Fig. 23). Streptavidin-horseradish peroxidase-$Cu_3(PO_4)_2$ nanoflowers have been synthesized and combined with immunosorbent assay and afterwards used for protein detection (Liu et al. 2017).

7.3 Nanourchins

This particular type of nanoparticles is characterized by long, thin spikes coming out of the central part of nanoparticle. Although they are sometimes called nanoviruses, nanohedgehogs or nanoflowers, their morphology is clearly different from those described in the previous section.
One example of the nanourchin type of structures would be coral-like Zn doped SnO_2 nanoparticles (Fig. 24 a, b) synthesized using hydrothermal method and further verified as a possible candidate for dye sensitized solar cells. As the synthesis was performed in an elevated temperature and pressure, at first $ZnSn(OH)_6$ bipyramids are formed. As the synthesis proceeds, bipyramids are then decomposed through OH^- etching and reformed as a crystalline wires springing from the etched plate left from the initial shape, see Fig. 24 c (Dou et al. 2011).
Slightly different, AuAg bimetallic nanourchins could be easily synthesized from the solution of gold tetrachloride, silver nitrate and ascorbic acid (Fig. 25). In this case, ascorbic acid acts here as a reducing agent for the metal ions. When gold particles precipitate, silver adsorbs on their surface selectively modifying their further growth. As a result, nanoparticles with clearly defined pikes emerging from gold centre are obtained (Chen et al. 2012). These kind of nanoparticles can be used as SERS active substrates as well as in biomedical applications.

8 Heterostructures

Different nanostructures, namely nanotubes, nanowires or nanoparticles were described so far. However, one may notice that their description was limited mostly to the structures composed of one specific chemical compound/single element. In here, the focus is put onto heterostructures that could be prepared from materials characterized with different properties than their counterparts. It should be here clarified also that by heterostructure we do not understand only "heterogeneous semiconductor structure built from two or more semiconductors, in such a way that the transition region or interface between the different materials plays an essential role in any device action" as was said by Herbert Kroemer during Nobel Lecture given on December 8th, 2000, but every structure composed of at least two various materials of different physical/chemical nature. Hetero-, composite and hybrid structure will be used as synonyms.
The obvious examples of composite materials are various kinds of nanoparticles, nanowires or nanowalls. Due to the structural features they can be divided into following categories: (i) simple hybrids (e.g. quantum dots, bimetallic nanoparticles), (ii) core-shell structures and (iii) functionalized complex systems (e.g. nanoflowers). As almost all groups of such structures have been already discussed, only quantum dots will be described in this part. Nevertheless, by hybrid nanostructure one can also understand different classes of nanomaterials combined together: e.g. zero-dimensional and three-dimensional. The classification of exemplary heterostructure materials is shown in Fig. 26. As only in 2018 more than 166000 scientific papers were published in the field of nanotechnology

(https://statnano.com/news/65056), one should take into account that only few selected examples will be referred in here.

8.1 Quantum nanodots

It is well known and accepted that quantum nanodots (QD) can be considered as the representative example of heterostructures. They are typically not only composed of two different materials but also QD can be regarded as semiconductors. Such nanocrystals were first discovered in the early 1980's by Alexey Ekimov and Louis Brus in glass matrix and colloidal solutions, respectively (Ekimov et al. 1985, Brus 1984)[,]. Generally, QD can be divided into six groups that corresponds to the groups of periodic table of elements: (i) IV (e.g. GeSn), (ii) IV-VI (e.g. PbS, PbTe), (iii) III-V (e.g. InAs, InSb), (iv) II-VI (e.g. HgCdTe, HgSe), (v) I-VI (e.g. Ag_2S, Ag_2Se) and (vi) I-III-VI (e.g. $CuInS_2$, $CuInSe_2$) (Lu et al. 2019). There are two usually used approaches for fabrication of QD: (i) solution synthesis, in which control over nucleation and growth of the nanoparticle can be assured and (ii) nanoscale pattering (mostly lithography based technologies) and epitaxial growth onto the particular substrate (Nozik et al. 2010). Nevertheless, it should be remembered that in the wet chemical route the hot solvents are used and therefore such a method is limited by the boiling temperature of the solution. While in the case of the latter approach, the system composed of QD and supporting platform can be hardly described as self-standing. However, for application purposes QD can be applied both in colloidal solution and in immobilized form. Due to their unique properties such as: (i) well defined composition, (ii) large bandgap tenability, (iii) bright emission response, (iv) photostability and (v) high selectivity towards targeted material, QD found applications in wide range of fields. It should be also underlined that Quantum Dots Market was valued to be 316 million USD in 2013 and is expected to reach over 5040 million USD in 2020 (https://www.alliedmarketresearch.com/quantum-dots-market). The possible applications of QD are presented in Fig. 27.

8.2 Dimensional hybrid nanostructures

As mentioned before zero-, one-, two- and three-dimensional structures can be combined with each other forming much more complex structures. Such combination allows for overcoming limitations of single materials. From strict economical point of view, the biggest limitation of materials is their price. For example taking into account only noble metal NPs, like Au, Ag, or Pt one can agree that they are quite expensive especially in terms of their practical applications. Therefore, the effort is put to combine them with e.g. metal oxides such as TiO_2, CeO_2, ZnO or WO_3 (Lin et al. 2009, Tanaka et al. 2014, Zhang et al. 2014, Primo et al. 2011). Such material, i.e. 0-D/0-D material, is the simplest example of dimensional heterostructures. Of course, omitting the economic aspect, the works are also focusing onto the preservation of properties of individual parts of heterostructures as well as the overall performance of prepared material. Moreover, it should not be forgotten that synergistic effect can lead to the fabrication of materials characterized by superior functionality and improved properties comparing to the counterparts. Therefore, it can be understood that heterostructures find their applications in the same areas of nanotechnology, as their single counterparts, e.g. in photovoltaic devices, batteries, supercapacitors, sensors, surface enhanced Raman scattering platforms or fuel cell.

One of the most represented groups seems to be 0-D/2-D structures. The obvious examples of such materials are: nanoparticles located at the thin film. The most common shape of nanoparticles is spherical or nearly spherical as it is the easiest

one to obtain as free energy of such system is minimal. Nevertheless, more visually interesting are nanoparticles of different shapes. For instance, Lewis et al. (2014) explored triangle cobalt nanoparticles over a copper support (Fig. 28).
Even more attractive example is reported by Lai et al. (2017) The researchers studied star-shaped Au/Ag NPs deposited onto silver film as a SERS substrate (Fig. 29) proving that such structures possess improved sensing properties.
On the other hand, less obvious configuration is the opposite one, i.e. 2-D material located onto 0-D one. Ji et al. (2012) worked onto silica microcapsules composed of flake-shells. Under hydrothermal synthesis conditions, silica spherical nanoparticles slowly dissolve and those dissolved silicate species form flakes surrounding the maintained spheres - see Fig. 30. Nevertheless, it should be noted that prolonged fabrication process leads to the creation of completely hollow spheres covered with flakes that can be used as capsules for drug delivery.
Another rich group of hybrid materials contains 3-D structures. For example Kim and Jeon et al. (2017) reported on fabrication of 3-D/2-D hybrid nanostructures composed of Au particles and cylindrical patterns onto indium tin oxide substrate (Fig. 31). It is stated that surface-structuring processes do not impact onto initial properties of the support and after covering with polymeric material obtained structures could be potentially applied in photovoltaics devices.
Other interesting example of 3-D heterostructure was given by Ke et al. (2015). The authors prepared TiO_2@$Ni(OH)_2$ core-shell nanostructures onto carbon fiber paper (Fig. 32) for supercapacitors applications. The prototype device was fabricated and the potential strategy to enhanced properties of battery type electrode was also introduced.
Material that can be used in energy storage was also reported by Xiong et al. (2018). Hybrid carbon nanotubes/gold nanoparticles structures were prepared (Fig. 33) and studied as active materials for efficient supercapacitors and templates for pseudocapacitors. It should be in here underlined that, inspired by nature authors called their electrodes: leaves-on branched structure.
Quite interestingly, nature is not a single source of inspiration for scientists. Human-created architecture can also influence the shape of the structures. For instance, Flomin et al. (2014) synthesized metal-ZnO hybrid nanopyramids with possibility to attach metallic nanoparticle to the base or the ZnO tip (Fig. 34) and obtained material was shown to be used as a promising nanocatalyst.
Above, just a few examples of various heterostructures were given. With schematic illustrations, SEM or TEM images, also possible applications were quoted. Nevertheless, the authors would like to finish this chapter with one more interesting material. Abellan et al. (2016) reported on hybrid material consisting of cadmium coordination polymer and NiAl-layered double hydroxide (Fig. 35). It is stated in this work that "with appropriate selection of building blocks, it is possible to engineer the assembly of different nanomaterials while keeping their initial functionalities intact." This sentence is an essence of motivation behind all studies on hybrid nanostructures. It can be said without any doubt that this field of science has not reached its limitation. Therefore, it is expected more works to be published in the future showing materials that will outperform the present ones.

References

E. Abbasi, S. F. Aval, A. Akbarzadeh, M. Milani, H. T. Nasrabadi, S. W. Joo, Y. Hanifehpour, K. Nejati-Koshki, R. Pashaei-Asl, Dendrimers: synthesis, applications, and properties, Nanoscale Research Letters 9 (2014) 247-257 https://doi.org/10.1186/1556-276X-9-247

G. Abellan, P. Amo-Ochao, J. L. G. Fierro, A. Ribera, E. Coronado, F. Zamora, Self-assembly of 1D/2D hybrid nanostructures consisting of a Cd(II) coordination polymer and NiAl-layered double hydroxides, Polymers 8 (2016) 5, 13. https://doi.org/ 10.3390/polym8010005

S. Ali, S. Hannula, Titania nanotube powders obtained by rapid breakdown anodization in perchloric acid electrolytes, Journal of Solid State Chemistry 249 (2017) 189-198, https://doi.org/10.1016/j.jssc.2017.03.007

K. Ariga, S. Watanabe, T. Mori, J. Takeya, Soft 3D nanoarchitecures, NPG Asia materials 10 (2018) 90-106, https://doi.org/10.1038/s41427-018-0022-

C. Arunchandran, S. Ramya, R. P. George, U. Kamachi Mudali, Corrosion inhibitor storage and release property of TiO_2 nanotube powder synthesized by rapid breakdown anodization method, Materials Research Bulletin 48 (2013) 635-639, https://doi.org/10.1016/j.materresbull.2012.11.034

F. Benz, R. Chikkaraddy, A. Salmon, H. Ohadi, B. de Nijs, J. Mertens, C. Carnegie, R.W. Bowman, J.J. Baumberg, SERS of Individual Nanoparticles on a Mirror: Size Does Matter, but so Does Shape, Journal Physical Chemistry Letters 7 (2016) 2264-2269, https://pubs.acs.org/doi/10.1021/acs.jpclett.6b00986

A. Berg, P. Caroff, N. Shahid, M.N. Lockrey, X. Yuan, M.T. Borgström, H.H. Tan, C. Jagadish, Growth and optical properties of $In_xGa_{1-x}P$ nanowires synthesized by selective-area epitaxy, Nano Research 10 (2017) 672-682. doi:10.1007/s12274-016-1325-1

S. R. Bhattarai, P. J. Derry, K. Aziz, P. K. Singh, A. M. Khoo, A. S. Chadha, A. Liopo, E. R. Zubarevc, S. Krishnan, Gold nanotriangles: scale up and X-ray radiosensitization effects in mice, Nanoscale 9 (2017) 5085-5093, doi: 10.1039/c6nr08172j

N. C. Bigall, T. Härtling, M. Klose, P. Simon, L. M. Eng, and A. Eychmüller, Monodisperse Platinum Nanospheres with Adjustable Diameters from 10 to 100 nm: Synthesis and Distinct Optical Properties, Nano Letters 8 (2008) 4588-4592, https://pubs.acs.org/doi/10.1021/nl802901t

S. Biswas, J. Doherty, D. Saladukha, Q. Ramasse, D. Majumdar, M. Upmanyu, A. Singha, T. Ochalski, M.A. Morris, J.D. Holmes, Non-equilibrium induction of tin in germanium: towards direct bandgap Ge1−xSnx nanowires, Nature Communications. 7 (2016) 11405. doi:10.1038/ncomms11405

S. Biswas, S. Barth, J.D. Holmes, Inducing imperfections in germanium nanowires, Nano Research 10 (2017) 1510-1523, doi:10.1007/s12274-017-1430-9

A. L. Beaudry, R. T. Tucker, J. M. LaForge, M. T. Taschuk, M. J. Brett, Indium tin oxide nanowhisker morphology control by vapour-liquid-solid glancing angle deposition, Nanotechnology 23 (2012) 105608, doi: 10.1088/0957-4484/23/10/105608

A.W. Bosman, H.M. Janssen, E.W. Meijer, About Dendrimers: Structure, Physical Properties, and Applications, Chemical Review 99 (1999) 1665-1688, https://pubs.acs.org/doi/10.1021/cr970069y

L.E. Brus, Electron-electron and electron-hole interactions is small semiconductor crystallites: the size dependence of the lowest excited electronic state, Journal of Chemical Physics 80 (1984) 4403.https://doi.org/10.1063/1.447218.

P.H. C. Camargo, K.G. Satyanarayana, F. Wypych, Nanocomposites: synthesis, structure, properties and new application opportunities, Material Research 12 (2009) 1-39, http://dx.doi.org/10.1590/S1516-14392009000100002

N. Chen, J. Hou, K. Lu, Formation Mechanism of TiO_2 Nanotubes and Their Applications in Photoelectrochemical Water Splitting and Supercapacitors, Langmuir 29 (2013) 5911-5919, http://10.1021/la400586r

L.-C. Cheng, J.-H. Huang, H. M. Chen, T.-Ching Lai, K.-Y. Yang, R.-S.. Liu, M. Hsiao, C.-H. Chen, L.-J. He, D. P. Tsai, Seedless, silver-induced synthesis of star-shaped gold/silver bimetallic nanoparticles as high efficiency photothermal therapy reagent, Journal Materials Chemistry 22 (2012) 2244-2253, doi: 10.1039/C1JM13937A

X. Chia, M. Pumera, Characteristics and performance of two-dimensional materials for electrocatalysis, Nature Catalysis 1 (2018) 909-921. doi:10.1038/s41929-018-0181-7

K. Choi, S. Chang, Effect of structure morphologies on hydrogen gas sensing by ZnO nanotubes, Materials Letters 230 (2018) 48-52, https://doi.org/10.1016/j.matlet.2018.07.031

Y. Cui, D. van Dam, S.A. Mann, N.J.J. van Hoof, P.J. van Veldhoven, E.C. Garnett, E.P.A.M. Bakkers, J.E.M. Haverkort, Boosting Solar Cell Photovoltage via Nanophotonic Engineering, Nano Letters 16 (2016) 6467–6471. doi:10.1021/acs.nanolett.6b02971

L. Dai, S. Mo, Q. Qin, X. Zhao, N. Zheng, Carbon Monoxide-Assisted Synthesis of Ultrathin PtCu 3 Alloy Wavy Nanowires and Their Enhanced Electrocatalysis, Small. 12 (2016) 1572-1577. doi:10.1002/smll.201502741

E. Dai, J. Xu, J. Qiu, S. Liu, P. Chen, Y. Liu, Co@Carbon and Co_3O_4@Carbon nanocomposites derived from a single MOF for supercapacitors, Science Reports 7 (2017) 12588. doi:10.1038/s41598-017-12733-5

X. Dou, D. Sabba, N. Mathews, L. H. Wong, Y. M. Lam, S. Mhaisalkar, Hydrothermal Synthesis of High Electron Mobility Zn-doped SnO_2 Nanoflowers as Photoanode Material for Efficient Dye-Sensitized Solar Cells, Chemistry Materials 23 (2011) 3938-3945, https://pubs.acs.org/doi/abs/10.1021/cm201366z

A.M. Ealias, M.P. Saravanakumar, A review on the classification, characterisation, synthesis of nanoparticles and their application, IOP Conference Series: Materials Science and Engineering 263 (2017) 032019, https://doi.org/10.1088/1757-899X/263/3/032019

A.I. Ekimov, Al. L. Efros, A. A. Onushchenko, Quantum size effect in semiconductor microcrystals, Solid State Communications 56 (1985) 921-924. https://doi.org/10.1016/S0038-1098(85)80025-9

K. Flomin, I. J-L. Plante, B. Moshofsky, M. Diab, T. Mokari. Selective growth of metal particles on ZnO nanopyramids via a one-pot synthesis, Nanoscale 6 (2014) 1335-1339. https://doi.org/ 10.1039/C3NR05661A.

L. Fu, C.L. Kane, Superconducting Proximity Effect and Majorana Fermions at the Surface of a Topological Insulator, Physical Review Letters 100 (2008) 096407. doi:10.1103/PhysRevLett.100.096407

S. Gangadoo, D. Stanley, R. J. Hughes, R. J. Moore, J. Chapman, The synthesis and characterisation of highly stable and reproducible selenium nanoparticles, Inorganic and Nano-Metal Chemistry 47 (2017) 1568-1576, https://doi.org/10.1080/24701556.2017.1357611

D van Gough, A. T. Juhl. P.V. Braun, Programming structure into 3D nanomaterials, Materials Today 12 (2009) 28-35, https://doi.org/10.1016/S1369-7021(09)70178-6

D. Gong, C. A. Grimes, O. K. Varghese, W. Hu, R. S. Singh, Z. Chen, E. C. Dickey, Titanium oxide nanotube arrays prepared by anodic oxidation, Journal of Materials Research 16 (2001) 3331-3334, https://doi.org/10.1557/JMR.2001.0457

J. Greeley, I.E.L. Stephens, A.S. Bondarenko, T.P. Johansson, H.A. Hansen, T.F. Jaramillo, J. Rossmeisl, I. Chorkendorff, J.K. Nørskov, Alloys of platinum and early transition metals as oxygen reduction electrocatalysts, Nature Chemistry. 1 (2009) 552–556. doi:10.1038/nchem.367

T. Haggren, A. Shah, A. Autere, J.-P. Kakko, V. Dhaka, M. Kim, T. Huhtio, Z. Sun, H. Lipsanen, Nanowire encapsulation with polymer for electrical isolation and enhanced optical properties, Nano Res. 10 (2017) 2657-2666. doi:10.1007/s12274-017-1468-8

R. Hahm, J. M. Macak, P. Schmuki, Rapid anodic growth of TiO_2 and WO_3 nanotubes in fluoride free electrolytes, Electrochemistry Communications 9 (2007) 947-952, https://doi.org/10.1016/j.elecom.2006.11.037

Z. Han, A. Fina, Thermal conductivity of carbon nanotubes and their polymer nanocomposites: A review, Progress in Polymer Science 36 (2011) 914-944, https://doi.org/10.1016/j.progpolymsci.2010.11.004

T. Han, A. Nag, S. C. Mukhopadhyay, Y. Xu, Carbon nanotubes and its gas-sensing applications: A review, Sensors and Actuators A: Physical 291 (2019) 107-143, https://doi.org/10.1016/j.sna.2019.03.053

A.N. Hattori, H. Nakazawa, T. Nakamura, H. Tanaka, Fabrication of the electric double layer transistor with (La,Pr,Ca)MnO_3 nanowall wire channel, Mod. Phys. Letters B 32 (2018) 1840058. doi:10.1142/S0217984918400584

R. Hu, X. Zhang, Z. Zhao, G. Zhu, T. Chen, T. Fu, W. Tan, DNA Nanoflowers for Multiplexed Cellular Imaging and Traceable Targeted Drug Delivery, Angewandte Chemie International Edition 53 (2014) 5821-5826, https://doi.org/10.1002/anie.201400323

Z. Hu, S. Li, P. Cheng, W. Yu, R. Li, X. Shao, W. Lin, D. Yuan, N,P-co-doped carbon nanowires prepared from bacterial cellulose for supercapacitor, Journal of Materials Science 51 (2016) 2627–2633 doi10.1007/s10853-015-9576-x

J. Huang, K. Zhang, Y. Lai, Fabrication, Modification, and Emerging Applications of TiO_2 Nanotube Arrays by Electrochemical Synthesis: A Review, International Journal of Photoenergy 2013 (2013) 1-19, https://doi.org/10.1155/2013/761971

X. Huang, P. Zhang, E. Lin, P. Wang, M. Mei, Q. Huang, J. Jiao, Q. Zhao, Fabrication and optically pumped lasing of plasmonic nanolaser with regular ZnO/GaN nanoheterojunction array, Applied Physics A 123 (2017) 605. doi:10.1007/s00339-017-1211-z

Y. Ichikawa, S. Yoshiba, M. Hirai, M. Konagai, Fabrication of Two-Dimensional Quantum Well Structure Consisting of Vertical Si Nano-Wall Arrays, Journal of The Electrochemical Society 164 (2017) H293-H298. doi:10.1149/2.0251706jes

Q. Ji, C. Guo, X. Yu, C. J. Ochs, J. P. Hill, F. Caruso, H. Nakazawa, K. Ariga, Flake shell capsules: adjustable inorganic structures, Small 8 (2012) 2345-2349. https://doi.org/10.1002/smll.201200317

S. G. Jiji, K. G. Gopchandran, Virus shaped gold nanoparticles with tunable near infrared plasmon as SERS substrates, Materials Research Express, 2 (2015) 075005

S. Iijima, Helical microtubules of graphitic carbon, Nature 354 (1991) 56-58, http://10.1038/354056a0

Q. Ke, M. Zheng, H. Liu, C. Guan, L. Mao, J. Wang, 3D TiO_2@$Ni(OH)_2$ core-shell arrays with tunable nanostructure for hybrid supercapacitor application, Nature Scientific Reports 5 (2015) 13940. https://doi.org/10.1038/srep13940

I. Khan, K. Saeed, I. Khan, Nanoparticles: Properties, applications and toxicities, Arabian Journal of Chemistry, 2017, doi.org/10.1016/j.arabjc.2017.05.011

J. Kim, W.J. da Silva, A.R. bin Mohd Yusoff, J. Jang, Organic devices based on nickel nanowires transparent electrode, Scientific Reports. 6 (2016) 19813. doi:10.1038/srep19813

S.-H. Kim, G.-I. Shim, S.-Y. Choi, Fabrication of Nb-doped ZnO nanowall structure by RF magnetron sputter for enhanced gas-sensing properties, Journal of Alloys and Compounds. 698 (2017) 77-86. doi:10.1016/j.jallcom.2016.11.377

J. W. Kim, H-J. Jeon, C-L, Lee, C. W. Ahn, Fabrication of three-dimensional hybrid nanostructure-embedded ITO and its application as a transparent electrode for high-efficiency solution processable organic photovoltaic devices, Nanoscale 9 (2017) 3033-3039. https://doi.org/ 10.1039/c6nr06552.
S.-W. Kim, K.-S. Kim, M. Park, W. Nah, D.U. Kim, C.-R. Lee, S.-B. Jung, J.-W. Kim, 1.4 μm-Thick Transparent Radio Frequency Transmission Lines Based on Instant Fusion of Polyethylene Terephthalate Through Surface of Ag Nanowires, Electronic Materials Letters. 14 (2018) 599–609. doi:10.1007/s13391-018-0069-3
C. Koenigsmann, D.B. Semple, E. Sutter, S.E. Tobierre, S.S. Wong, Ambient Synthesis of High-Quality Ruthenium Nanowires and the Morphology-Dependent Electrocatalytic Performance of Platinum-Decorated Ruthenium Nanowires and Nanoparticles in the Methanol Oxidation Reaction, ACS Appl. Mater. Interfaces. 5 (2013) 5518–5530. doi:10.1021/am4007462
S. Kumar, R. Rani, N. Dilbaghi, T. Tankeshwar, K. Kim, Carbon nanotubes: a novel material for multifaceted applications in human healthcare, Chemical Society Reviews 46 (2017) 158-196, http://10.1039/C6CS00517A
C. H. Lai, G-A. Wang, T-K. Ling, T-J. Wang, P-K. Chiu, Y-F. C Chau, C-C. Huang, H-P. Chiang, Near infrared surface-enhanced Raman scattering based on star-shaped gold/silver nanoparticles and hyperbolic metamaterial, Scientific Reports 7 (2017) 5446, https://doi.org/10.1038/s41598-017-05939-0
H. B. Lee, Y. M. Yoo, Y-H. Han, Characteristic optical properties and synthesis of gold-silica core-shell colloids, Scripta Materialia 55 (2006) 1127-1129, doi: 10.1016/j.scriptamat.2006.08.044
W. Lee, K. Schwirn, M. Steinhart, E. Pippel, R. Scholz, U. Gosels, Structural engineering of nanoporous anodic aluminium oxide by pulse anodization of aluminium, Nature Nanotechnology 3 (2008) 234-239, https://doi.org/10.1038/nnano.2008.54
K. Lee, A. Mazare, P. Schmuki, One-Dimensional Titanium Dioxide Nanomaterials: Nanotubes, Chemical Reviews 114 (2014) 9385-9454, http:// 10.1021/cr500061m
W. Lee, Park S., Porous Anodic Aluminum Oxide: Anodization and Templated Synthesis of Functional Nanostructures, Chemical Reviews 114 (2014) 7487-7556, http://10.1021/cr500002z
A. Lekawa-Raus, J. Patmore, Ł. Kurzepa, J. Bulmer, K. Kozioł, Electrical Properties of Carbon Nanotube Based Fibers and Their Future Use in Electrical Wiring, Advanced Functional Materials 24 (2014) 3661-3682, https://doi.org/10.1002/adfm.201303716
C.M. Lentz, B.A. Samuel, H.C. Foley, M.A. Haque, Synthesis and Characterization of Glassy Carbon Nanowires, Journal of Nanomaterials 2011 (2011) 1-8. doi:10.1155/2011/129298
E. A. Lewis, M. D. Marcinkowski, C. J. Murphy, M. L. Liriano, E. C. H. Sykes, Hydrogen dissociation, spillover, and desorption from Cu-supported Co nanoparticles, Journal of Physical Chemistry Letters 5 (2014) 3380-3385. https://doi.org/10.1021/jz5016789.
W.-C. Lin, W.-D. Yang, I.-L. Huang, T.-S. Wu, Z.-J. Chung, Hydrogen production from methanol/water photocatalytic decomposition using Pt/$TiO_{2-x}N_x$ catalyst, Energy Fuels 23 (2009) 2192-2196. https://doi.org/ 10.1021/ef801091p.
X. Liu, M. Atwater, J. Wang, Q. Huo, Extinction coefficient of gold nanoparticles with different sizes and different capping ligands, Colloids and Surfaces B: Biointerfaces 58 (2007) 3-7, doi: 10.1016/j.scriptamat.2006.08.044
J. Liu, S. Z. Qiao, J. S. Chen, X. W. Lou, X. Xing, G. Q. Lu, Yolk/shell nanoparticles: new platforms for nanoreactors, drug delivery and lithium-ion

batteries, Chemistry Commununications 47 (2011) 12578, doi: 10.1039/C1CC13658E
R. Liu, J. Duay, S. B. Lee, Heterogeneous nanostructured electrode materials for electrochemical energy storage, Chemical Communications 47 (2011) 1384-1404. https://doi.org/ 10.1039/C0CC03158E
Y. Liu, J. Chen, M. Du, X. Wang, X. Ji, Z. He, The preparation of du-al-functional hybrid nanoflower and its application in the ultrasensitive detection of disease-related biomarker, Biosensors and Bioelectronics 92 (2017) 68-73, doi: 10.1016/j.bios.2017.02.004
D. Liu, C. Zhang, Y. Yu, Y. Shi, Y. Yu, Z. Niu, B. Zhang, Hydrogen evolution activity enhancement by tuning the oxygen vacancies in self-supported mesoporous spinel oxide nanowire arrays, Nano Research 11 (2018) 603-613. doi:10.1007/s12274-017-1670-8
J. Long, W. Wang, S. Fu, L. Liu, Hierarchical architectures of wrinkle-like $ZnFe_2O_4$ nanosheet-enwrapped ZnO nanotube arrays for remarkably photoelectrochemical water splitting to produce hydrogen, Journal of Colloid and Interface Science 536 (2019) 408-413, https://doi.org/10.1016/j.jcis.2018.10.074
H. Lu, G. M. Carroll, N. R. Neale, M. C. Beard, Infrared quantum dots: progress, challenges and opportunities, ACS Nano 13 (2019) 939-953. https://doi.org/ 10.1021/acsnano.8b09815
J. M. Macak, S. P. Albu, P. Schmuki, Towards ideal hexagonal self- ordering of TiO_2 nanotubes, Physica Status Solidi 1 (2007) 181-183, https://doi.org/10.1002/pssr.200701148
D. E. Manolopoulos, P. W. Fowler, Structural proposals for endohedral metal-fullerene complexes, Chemical Physical Letters 187 (1991) 1-7, https://doi.org/10.1016/0009-2614(91)90475-O
I.S. Merenkov, M.S. Myshenkov, Y.M. Zhukov, Y. Sato, T.S. Frolova, D.V. Danilov, I.A. Kasatkin, O.S. Medvedev, R.V. Pushkarev, O.I. Sinitsyna, M. Terauchi, I.A. Zvereva, M.L. Kosinova, K. Ostrikov, Orientation-controlled, low-temperature plasma growth and applications of h-BN nanosheets, Nano Research 12 (2019) 91-99. doi:10.1007/s12274-018-2185-7
A. Mikkelsen, E. Lundgren, Surface science of free standing semiconductor nanowires, Surface Science 607 (2013) 97-2015, doi: 10.1016/j.susc.2012.08.002
A. Mohamed, Chapter Eight - Synthesis, Characterization and Applications Carbon Nanofibers, Carbon-Based Nanofillers and Their Rubber Nanocomposites (2019) 243-257, https://doi.org/10.1016/B978-0-12-813248-7.00008-0
J.E. Mooij, G. Schön, A. Shnirman, T. Fuse, C.J.P.M. Harmans, H. Rotzinger, A.H. Verbruggen, Superconductor–insulator transition in nanowires and nanowire arrays, New Journal of Physics. 17 (2015) 033006. doi:10.1088/1367-2630/17/3/033006
V. Mourik, K. Zuo, S.M. Frolov, S.R. Plissard, E.P. A. M. Bakkers, L.P. Kouwenhoven, Signatures of Majorana Fermions in Hybrid Superconductor-Semiconductor Nanowire Devices, Science 336 (2012) 1003-1007. doi:10.1126/science.1222360
P. Mroz, A. Pawlak, M. Satti, H. Lee, T. Wharton, H. Gali, T. Sarna, M. R. Hamblin, Functionalized fullerenes mediate photodynamic killing of cancer cells: Type I versus Type II photochemical mechanism, Free Radical Biology and Medicine 43 (2007) 1139-1149, doi: 10.1016/j.freeradbiomed.2007.05.005
A. J. Nozik, M. C. Beard, J. M. Luther, M. Law, R. J. Ellingson, J. C. Johnson, Semiconductor quantum dots and quantum dots arrays and applications of multiple excitation generation to third-generation photovoltaic solar cells, Chemical Reviews 110 (2010) 6873-6890. https://doi.org/ 10.1021/cr900289f

S. Ozkan, N. T. Nguyen, A. Mazare, P. Schmuki, Optimized Spacing between TiO_2 Nanotubes for Enhanced Light Harvesting and Charge Transfer, ChemElectroChem 5 (2018) 1-9, https://doi.org/10.1002/celc.201801136

M. Paradise, T. Goswami, Carbon nanotubes - Production and industrial applications, Materials and Design 28 (2007) 1477-1489, https://doi.org/10.1016/j.matdes.2006.03.008

VV. Pokropivny, VV. Skorokhod, Classification of nanostructures by dimensionality and concept of surface forms engineering in nanomaterial science, Materials Science and Engineering. C, Biomimetic Materials, Sensors and Systems 27 (2007) 990-993, http://dx.doi.org/10.1016/j.msec.2006.09.023

A. Primo, T. Marino, A. Corma, R. Molinari, H. García, Efficient visible-light photocatalytic water splitting by minute amounts of gold supported on nanoparticulate CeO_2 obtained by a biopolymer templating method, Journal of American Chemical Society 133 (2011) 6930–6933. https://doi.org/ 10.1021/ja2011498

N. Ra. Je. Hynes, R. Sankaranarayanan, M. Kathiresan, P. Senthamaraikannan, Anish Khan, Abdullah Mohamed Asiri, Imran Khan, Synthesis, properties, and characterization of carbon nanotube-reinforced metal matrix composites, 27 - Nanocarbon and its Composites (2019) 805-830, https://doi.org/10.1016/B978-0-08-102509-3.00027-4

C. Radloff, N. J. Halas, Plasmonic Properties of Concentric Nanoshells, Nano Letters 4 (2004) 1323-1327, https://pubs.acs.org/doi/10.1021/nl049597x

V. R. Raphey, T. K. Henna, K. P. Nivitha, P. Mufeedha, Chinnu Sabu, K. Pramod, Advanced biomedical applications of carbon nanotube, Materials Science and Engineering: C 100 (2019) 616-630, https://doi.org/10.1016/j.msec.2019.03.043

D. Regonini, C. R. Bowen, A. Jaroenworaluck, R. Stevens, A review of growth mechanism, structure and crystallinity of anodized TiO_2 nanotubes, Materials Science and Engineering: R: Reports 74 (2013) 377-406, https://doi.org/10.1016/j.mser.2013.10.001

G. Reguera, K.D. McCarthy, T. Mehta, J.S. Nicoll, M.T. Tuominen, D.R. Lovley, Extracellular electron transfer via microbial nanowires, Nature 435 (2005) 1098. doi:10.1038/nature03661

P. Russo, M. Xiao, N.Y. Zhou, Carbon nanowalls: A new material for resistive switching memory devices, Carbon 120 (2017) 54-62 doi:10.1016/j.carbon.2017.05.004

P. Samadipakchin, Mortaheb H. R., Zolfaghari A., ZnO nanotubes: Preparation and photocatalytic performance evaluation, Journal of Photochemistry and Photobiology A: Chemistry 337 (2017) 91-99, https://doi.org/10.1016/j.jphotochem.2017.01.018

T. Sannicolo, M. Lagrange, A. Cabos, C. Celle, J.-P. Simonato, D. Bellet, Metallic Nanowire-Based Transparent Electrodes for Next Generation Flexible Devices: a Review, Small. 12 (2016) 6052-6075. doi:10.1002/smll.201602581

H. Seo, Y. Jung, S. Jee, J. M. Yang, J. Lee, Compositionally bilayered feature of interfacial voids in a porous anodic alumina template directly formed on Si, Scripta Materialia 57 (2007) 968-971, https://doi.org/10.1016/j.scriptamat.2007.06.067

W. Shen, J. Zhang, S. Wang, H. Du, Y. Tang, Improve the performance of the quantum dot sensitized ZnO nanotube solar cells with inserting ZnS-MnS composites layers, Journal of Alloys and Compounds 787 (2019) 751-758, https://doi.org/10.1016/j.jallcom.2019.02.108

J. T. Smith, Q. Hang, A. D. Franklin, D. B. Janes, T. D. Sands, Highly ordered diamond and hybrid triangle-diamond patterns in porous anodic alumina thin films, Applied Physics Letters 93 (2008) 1-3, https://doi.org/10.1063/1.2957991

A.G.N. Sofiah, M. Samykano, K. Kadirgama, R.V. Mohan, N.A.C. Lah, Metallic nanowires: Mechanical properties - Theory and experiment, Applied Materials Today. 11 (2018) 320–337. doi:10.1016/j.apmt.2018.03.004

G. D. Sulka, J. Kapusta-Kołodziej, A. Brzózka, M. Jaskuła, Fabrication of nanoporous TiO2 by electrochemical anodization, Electrochemica Acta 55 (2010) 4359-4367, https://doi.org/10.1016/j.electacta.2009.12.053

Y. Tan, R.Y. Adhikari, N.S. Malvankar, S. Pi, J.E. Ward, T.L. Woodard, K.P. Nevin, Q. Xia, M.T. Tuominen, D.R. Lovley, Synthetic Biological Protein Nanowires with High Conductivity, Small 12 (2016) 4481-4485. doi:10.1002/smll.201601112

A. Tanaka, K. Hashimoto, H. Kominami, Visible-light-induced hydrogen and oxygen formation over $Pt/Au/WO_3$ photocatalyst utilizing two types of photoabsorption due to surface plasmon resonance and band-gap excitation, Journal of American Chemical Society 136 (2014) 586-589. https://doi.org/ 10.1021/ja410230u

N. Tang, W. Wang, H. You, Z. Zhai, J. Hilario, L. Zeng, L. Zhang, Morphology tuning of porous CoO nanowall towards enhanced electrochemical performance as supercapacitors electrodes, Catalysis Today 330 (2019) 240-245 doi:10.1016/j.cattod.2018.03.024

S.J. Tans, M.H. Devoret, H. Dai, A. Thess, R.E. Smalley, L.J. Geerligs, C. Dekker, Individual single-wall carbon nanotubes as quantum wires, Nature 386 (1997) 474. doi:10.1038/386474a0

L. V. Taveira, J. M. Macak, H. Tsuchiya, L. F. P. Dick, P. Schmuki, Initiation and Growth of Self-Organized TiO_2 Nanotubes Anodically Formed in $NH_4F/(NH_4)_2SO_4$ Electrolytes, Journal of Electrochemical Society 152 (2005) B405-B410, http://10.1149/1.2008980

G. P. Tegos, T. N. Demidova, D. Arcila-Lopez, H. Lee, T. Wharton, H. Gali, M. R. Hamblin, Cationic fullerenes Are Effective and Selective Antimicrobal Photosensitizers, Chemistry & Biology 12 (2005) 1127-1135

M. Tian, J. Wang, W. Ning, T.E. Mallouk, M.H.W. Chan, Surface Superconductivity in Thin Cylindrical Bi Nanowire, Nano Letters 15 (2015) 1487-1492. doi:10.1021/nl503398d

J.N. Tiwari, R.N. Tiwari, K. S. Kim, Zero-dimensional, one-dimensional, two-dimensional and three-dimensional nanostructured materials for advanced energy devices, Progress in Materials Science 67 (2012) 724-803, doi:10.1016/j.pmatsci.2011.08.003

D. van Treeck, G. Calabrese, J.J.W. Goertz, V.M. Kaganer, O. Brandt, S. Fernández-Garrido, L. Geelhaar, Self-assembled formation of long, thin, and uncoalesced GaN nanowires on crystalline TiN films, Nano Res. 11 (2018) 565–576. doi:10.1007/s12274-017-1717-x

R. Wang, J. Tao, B. Yu, L. Dai, Characterization of multiwalled carbon nanotube-polymethyl methacrylate composite resins as denture base materials, The Journal of Prosthetic Dentistry 111 (2014) 318-326, https://doi.org/10.1016/j.prosdent.2013.07.017A.

Q. Wang, J. Huang, H. Li, A. Z. Zhao, Y. Wang, K. Zhang, H. Sun, Y. Lai, Recent advances on smart TiO2 nanotube platforms for sustainable drug delivery applications, International Journal of Nanomedicine 12 (2017) 151-165, https://doi.org/10.2147/IJN.S117498

G. Xiong, P He, Z. Lyu, T. Chen, B. Huang, L. Chen, T. S. Fisher, Bioinspired leaves-on-branchlet hybrid carbon nanostructure for supercapacitors, Nature Communications 9 (2018) 790. https://doi.org/10.1038/s41467-018-03112-3.

J. Yan, F. Zhou, TiO_2 nanotubes: Structure optimization for solar cells, Journal of Materials Chemistry 21 (2011) 9406-9418, http:// 10.1039/C1JM10274E

K. Yao, C. Zhao, N. Sun, W. Lu, Y. Zhang, H. Wang, J. Wang, Freestanding CuS nanowalls: ionic liquid-assisted synthesis and prominent catalytic performance for the decomposition of ammonium perchlorate, Cryst Eng Comm. 19 (2017) 5048-5057. doi:10.1039/C7CE01119A
S. Yi, L. Sun, S. C. Lenaghan, Y. Wang, X. Chong, Z. Zhang, M. Zhang, One-step synthesis of dendritic gold nanoflowers with high surface-enhanced Raman scattering (SERS) properties, RSC Advances 3 (2013) 10139-10144, doi: 10.1039/C3RA40716K
W.-J. Yin, X.-G. Gong, S.-H. Wei, Origin of the unusually large band-gap bowing and the breakdown of the band-edge distribution rule in the SnxGe1-x alloys, Physical Review B 78 (2008) 161203. doi:10.1103/PhysRevB.78.161203
X. Yu, X. Yu, J. Zhang, L. Chen, Y. Long, D. Zhang, Optical properties of conductive silver-nanowire films with different nanowire lengths, Nano Res. 10 (2017) 3706–3714. doi:10.1007/s12274-017-1583-6
J. Yun, M. Lee, Y. Jeon, M. Kim, Y. Kim, D. Lim, S. Kim, Nanowatt power operation of silicon nanowire NAND logic gates on bendable substrates, Nano Research 9 (2016) 3656–3662. doi:10.1007/s12274-016-1235-2
H. Zhai, Y. Li, L. Chen, X. Wang, L. Shi, R. Wang, J. Sun, Semi-transparent polymer solar cells with all-copper nanowire electrodes, Nano Research 11 (2018) 1956-1966. doi:10.1007/s12274-017-1812-z
W. Zhao, N. Du, C. Xiao, H. Wu, H. Zhang, D. Yang, Large-scale synthesis of Ag–Si core–shell nanowall arrays as high-performance anode materials of Li-ion batteries, J. Mater. Chem. A. 2 (2014) 13949–13954. doi:10.1039/C4TA03238A
L.L. Zhang, X. S. Zhao, Carbon-based materials as supercapacitor electrodes, Chemical Society Reviews 38 (2009) 2520-2531, http://10.1039/B813846J
X. Zhang, Y. Liu, Z. Kang, 3D branched ZnO nanowire arrays decorated with plasmonic Au nanoparticles for high-performance photoelectrochemical water splitting, ACS Applied Materials & Interfaces 6 (2014) 4480-4489. https://doi.org/10.1021/am500234v.
Y. Zhang, M. Liu, W. Ren, Z. Ye, Well-ordered ZnO nanotube arrays and networks grown by atomic layer deposition, Applied Surface Science 340 (2015) 120-125, https://doi.org/10.1016/j.apsusc.2015.02.176
K. Zhang, Y. Feng, F. Wang, Z. Yang, J. Wang, Two dimensional hexagonal boron nitride (2D-hBN): synthesis, properties and applications, Journal of Materials Chemistry C 5 (2017) 11992-12022. doi:10.1039/C7TC04300G
C. Zhang, C. Zheng, S. Zhou, Y. Shen, C. Zuo, Enhanced electrochromic porous cobalt oxides nanowall electrodes: A new way for fast modulation of yellow-brown light, Materials Research Bulletin 89 (2017) 204-209 doi:10.1016/j.materresbull.2017.01.037
K. Zhang, Y. Cai, C. Yao, X. Wen, Y. Han, H. Yin, W. Sun, Q. Li, Structures, growth mechanism and optical properties of Ag-ZnO cored nanotubes, Materials letters 234 (2019) 191-195, https://doi.org/10.1016/j.matlet.2018.09.100
F. Zhao, J.G. Zheng, X. Yang, X. Li, J. Wang, F. Zhao, K. S. Wong, C. Liang, M. Wu, Complex ZnO nanotree arrays with tunable top, stem and branch structures, Nanoscale 2 (2010) 1674-1683, https://doi.org/10.1039/C0NR00076K
M. Zhou, X.W. (David) Lou, Y. Xie, Two-dimensional nanosheets for photoelectrochemical water splitting: Possibilities and opportunities, Nano Today. 8 (2013) 598–618. doi:10.1016/j.nantod.2013.12.002
J. Zhu, Y.K. Sharma, Z. Zeng, X. Zhang, M. Srinivasan, S. Mhaisalkar, H. Zhang, H.H. Hng, Q. Yan, Cobalt Oxide Nanowall Arrays on Reduced Graphene Oxide Sheets with Controlled Phase, Grain Size, and Porosity for Li-Ion Battery

Electrodes, Journal of Physical Chemistry C 115 (2011) 8400-8406 doi:10.1021/jp2002113
A. K. Zulhairum, M. S. Abdullah, A. F. Ismail, P. S. Goh, Chapter 1 - Graphene and CNT Technology, Current Trends and Future Developments on (Bio-) Membranes (2019) 3-26, https://doi.org/10.1016/B978-0-12-813551-8.00001-2

http://www.software3d.com/Stella.php, Distributed under GNU General Public License, Created using Stella Software;
https://statnano.com/news/65056 (accessed 07.05.2019)
https://www.alliedmarketresearch.com/quantum-dots-market(accessed: 07.05.2019).

Tables

Table 1. Classification of nanomaterials depending on the dimensions.

0-D	1-D	2-D	3-D
nanoparticles, quantum dots (Elias and Saravanakumar, 2017)	nanotubes, nanorods, nanowires (Mikklesen and Lundgre, 2013)	nanofilms, nanolayers, nanocoatings (Ariga et al. 2018)	bundles of nanotubes, nanowires, multi-layered materials (van Gough etl al. 2009)
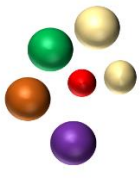	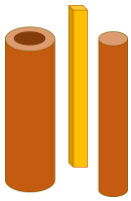	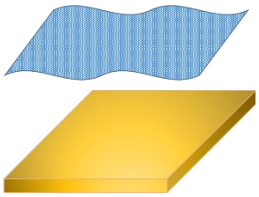	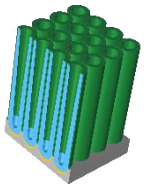

Table 2. Examples of top-down fabrication methods.

Litography methods	Methods requiring inexpensive energy consumption and expensive facilities; are based on making printed electric circuits and computer broads.
Anodization	Electrochemical oxidation of metal substrate performed usually in 2-electrode arrangement when both electrodes are immersed in the etching electrolyte. Electrodes are placed opposite to each other. Optimization of process parameters enables formation of porous layer composed of highly ordered aligned or separated nanotubes.
Mechanosynthetic method	The cheapest way to material fragmentation. Most common technique is ball milling based on the mechanical attrition when kinetic energy is transferred to bigger substrate undergoing destruction.
Thermal method	In general it concerns application of thermal stress to thin metallic films that upon elevated temperatures tend to form nanoislands/nanoparticles on the substrate. The thermal treatment could be realized in an electric oven or by the interaction with the laser beam.
Laser ablation	Laser light interacts with the solid target and kicks of ions that could then collide with each other and be deposited on the substrate or just imprisoned in medium when the target is immersed in liquid environment.

Table 3. Examples of bottom-up fabrication methods.

Chemical vapour deposition (CVD)	Occurs in gas phase where on the substrate surface the decomposition of precursors takes place and the desired nanostructure is formed. This method is usually applied for fabrication of carbon nanotubes or carbon like diamond.
Atomic layer deposition (ALD)	States as an industrial process that allows to coat uniformly material of any topography. In each deposition cycle, a monolayer or few are formed. Unfortunately, used precursors are of high cost.
Electrochemical deposition	Requires conductive substrate that can be polarized in a certain mode. Usually: potentiostatic or potentiodynamic (pulsed mode, cyclic voltammetry) techniques are applied to deposit the material onto the working electrode acting here as a substrate. The conductive electrolyte with easily dissolved material precursor is required. With the help of electrochemical deposition, the layers of conducting polymers, semiconductors or thin metallic films are formed.
Sol-gel	Regarded as a soft chemical process, usually applied for fabrication of metal oxides or ceramic materials. Depending on established conditions, spherical or tube shape, thin coatings, membranes could be obtained.

Table 4. The classification of nanostructures fabrication methods based on their chemical or physical character.

Physical techniques	**Chemical techniques**
Sputtering techniques, lithography process, hot and cold plasma, evaporation technique, spray pyrolysis, pulsed laser ablation, sonochemical reduction	Electrochemical deposition, lyotropic liquid crystal templates, hydrothermal and solvothermal techniques, sol-gel technique, chemical vapour deposition, laser pyrolysis

Table 5. Differences between SWCNTs and MWCNTs.

SWCNTs	MWCNTs
Single layer of graphene	Multiple layers of graphene
Catalyst is required for synthesis	Can be produced without catalyst
Bulk synthesis is difficult as it requires proper control over growth and atmospheric conditions	Bulk synthesis is easier
Purity is poor	Purity is high
High risk of defects during functionalization	Low risk of defects and if occurred, can be improved
Can be twisted easily due to a single later of graphene	Cannot be twisted easily due to multiple layers

Table 6. Brief summary of TiO_2 NTs evolution.

TiO_2 NTs generation	Electrolyte	Short description	SEM	Reproduced from
1st	aqueous HF solution	limited length to 0.5 µm; ribbed structure	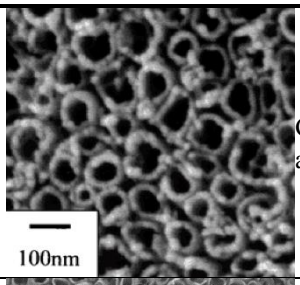	Gong et al. (2001)
2nd	buffered aqueous solutions with F^- ions	increased length compared to 1st gen. up to 5 µm; ribbed structure	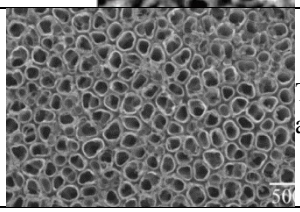	Taveira et al. (2005)
3rd	Ethylene glycol (EG) solution	increased length compared to 1st and 2nd generation up to 1000 µm; uniform and smooth layer of TiO_2 NTs	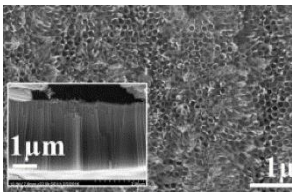	
	Diethylene glycol (DEG)	spaced NTs; not so uniform; ribs present at the bottom	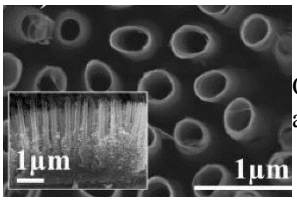	Ozkan et al. (2018)
	Dimethyl sulfoxide (DMSO)	spaced NTs; over-etched walls (compared to DEG); not so uniform; ribs at the bottom	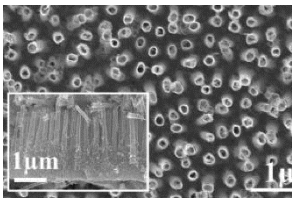	
4th	$HClO_4$ (fluoride-free solution)	non uniform structure; high aspect ratio achieved only within local areas	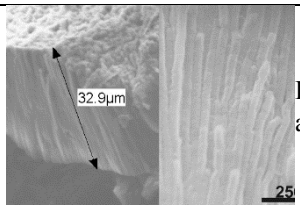	Hahm et al. (2007)

EG with optimized anodization parameters	highly ordered hexagonal structure	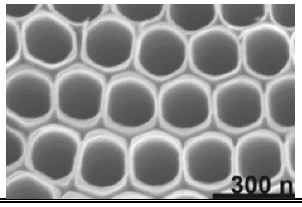

Figures

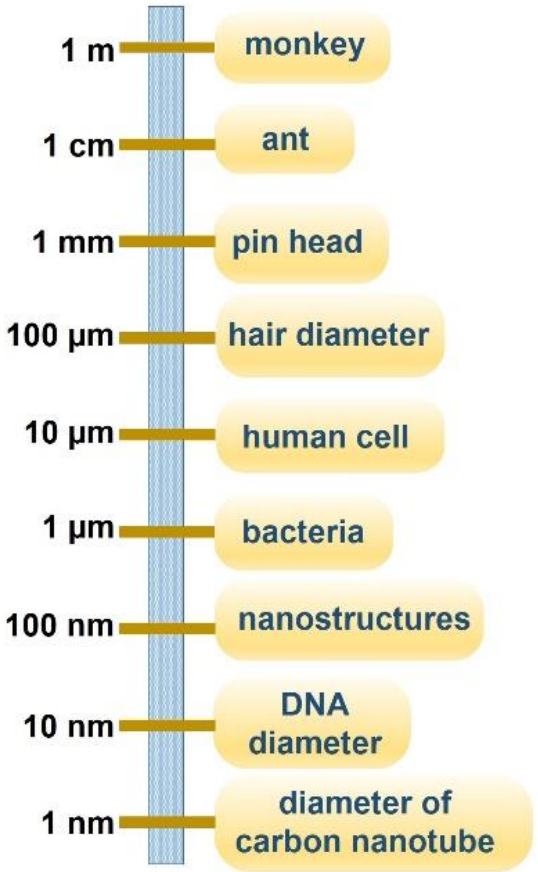

Fig. 1. Dimensions scale with the examples of objects from the 1 m to the 1 nm.

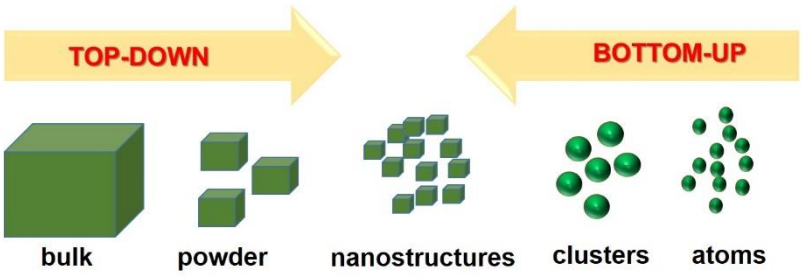

Fig. 2. The general scheme depicting the idea of bottom-up and top-down approaches for nanostructures synthesis.

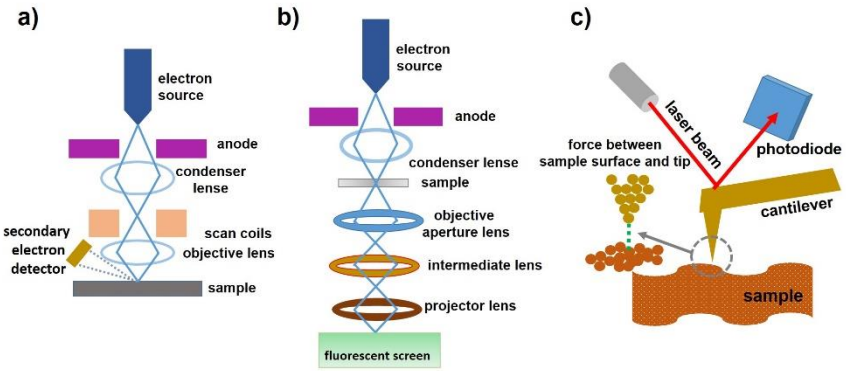

Fig. 3. The schemes depicting the operation principle of SEM (a), TEM (b) and AFM (c) microscopies utilized frequently to illustrate the morphology of nanostructures.

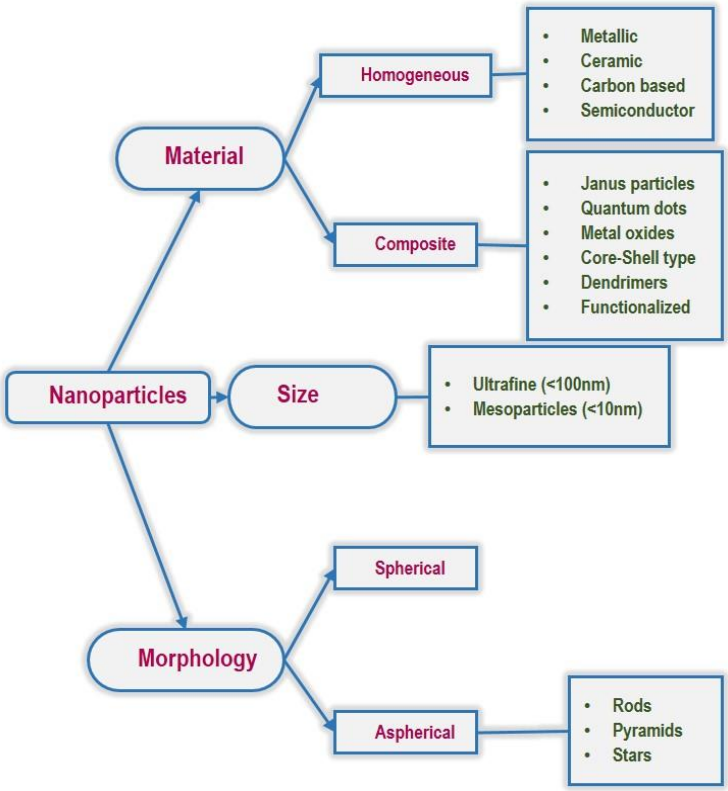

Fig. 4. General classification of nanoparticles.

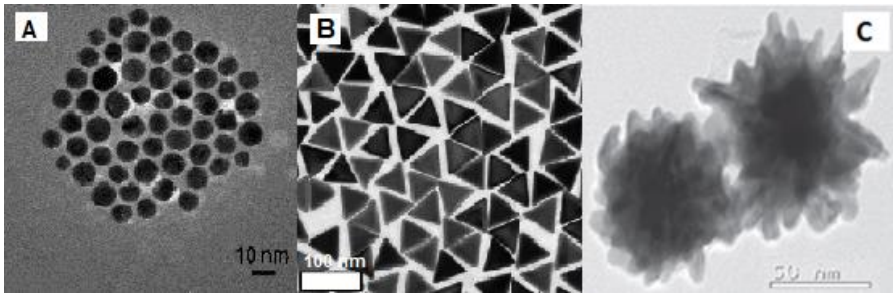

Fig. 5. Examples of gold nanoparticles synthesized through wet-chemistry methods. a) spherical NPs (Reproduced from Liu et al. 2007), b) triangular NPs (Reproduced from Bhattari et al. (2017), c) virus-shaped NPs. (Reproduced from Jiji and Gopchandran 2015).

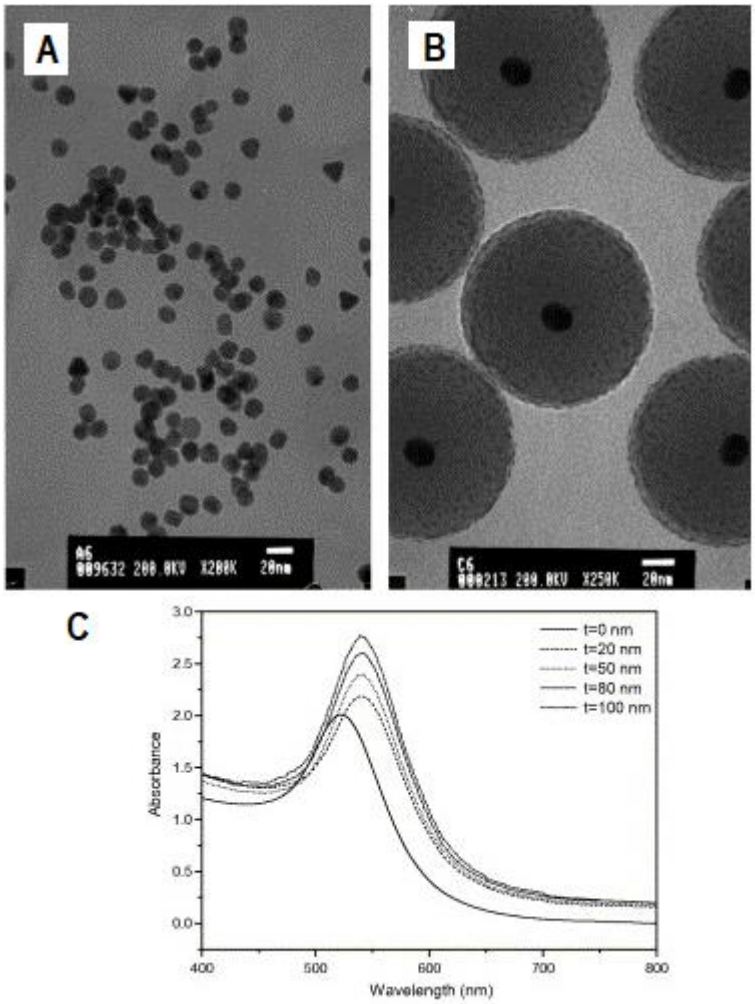

Fig. 6. Absorbance spectra of gold nanoparticles (A) is heavily dependent on the thickness of outer silica shell (B), therefore spectroscopical measurements (C) can be a useful tool for determining shell parameters. Reproduced from Lee et al. (2006).

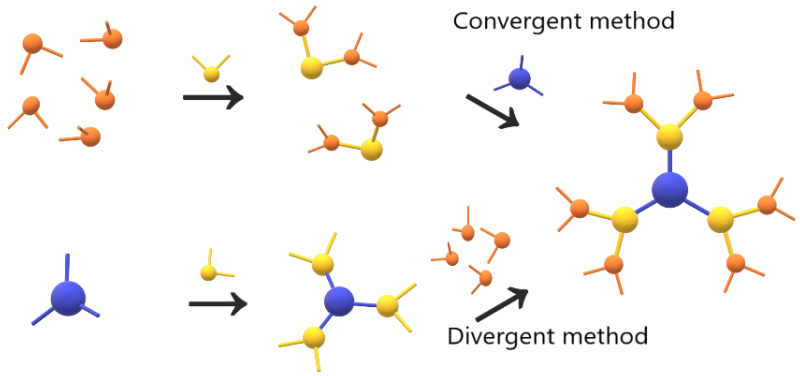

Fig. 7. Schematic representation of convergent and divergent methods of dendrimer synthesis.

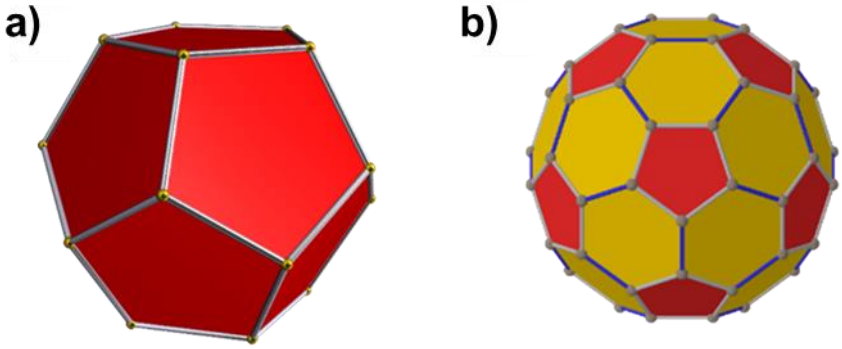

Fig. 8. Visual representation of the structure of C20 (a) and C60 fullerenes (b) Red colour indicates pentagonal planes, while yellow shows hexagonal planes. (created using Stella Softwar).

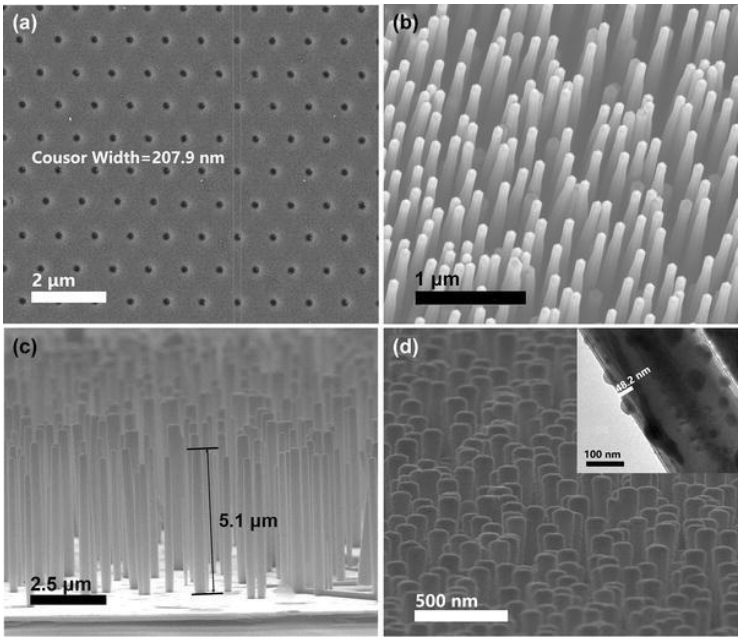

Fig. 9. SEM characterization of the structure used in laser based nanodevice: a) SEM image of a regular hexagonal array of nanoholes on the substrate, b) top view SEM image of n-type bare ZnO NWs (the diameter is of 120 ± 10 nm), c) side view SEM image of n-type vertically aligned ZnO NWs (the length is about 5.1 μm) array on the p-type GaN substrate, d) top view SEM image of n-type vertically aligned ZnO NWs, the inset is the TEM image of a single NW coated by a hybrid SiO_2/Ag film with a thickness of 50 nm. Reproduced from Huang el al. (2017).

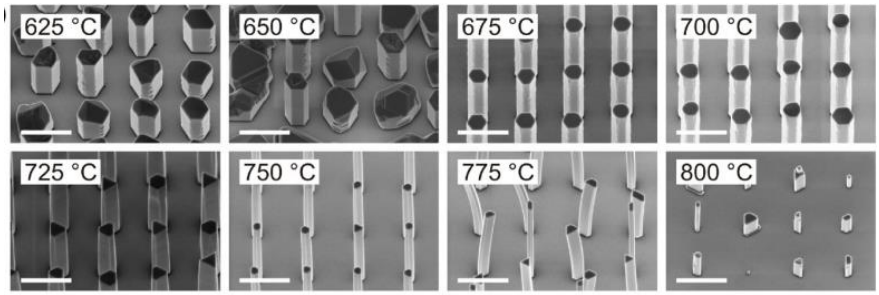

Fig. 10. The series of InGaP NWs for samples obtained under different thermal conditions. SEM images were obtained for the array with a 30 nm hole diameter and a 1 μm pitch. The scale bars are 1 μm. Reproduced from Berg et al. (2017).

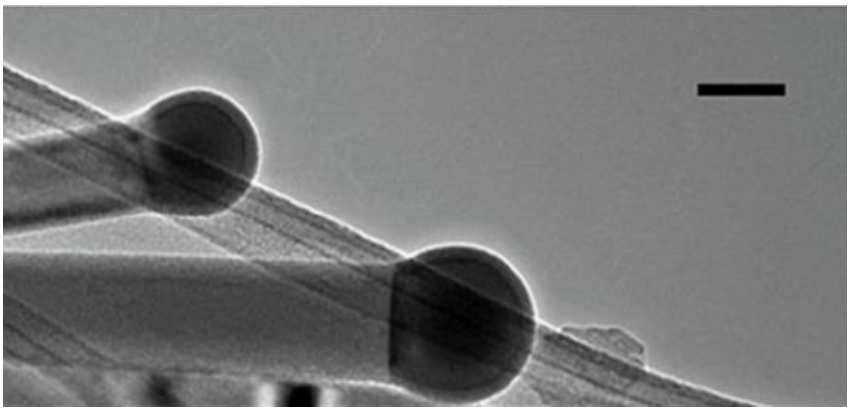

Fig. 11. TEM image confirming the participation of VLS growth mechanism with dark-contrast spherical seed at the tip of the nanowire with AuAg catalysts from precursor solution containing 15 at.% Sn. Scale bar is 100 nm. Reprinted with permission from. Reproduced from Biswas et al. (2016).

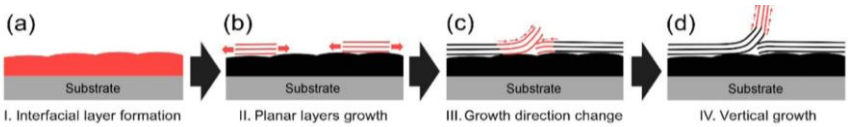

Fig. 12. Schematic representation of the h-BN nanowall growth mechanism. Reprinted with permission from. Reproduced from Merenkov et al. (2019).

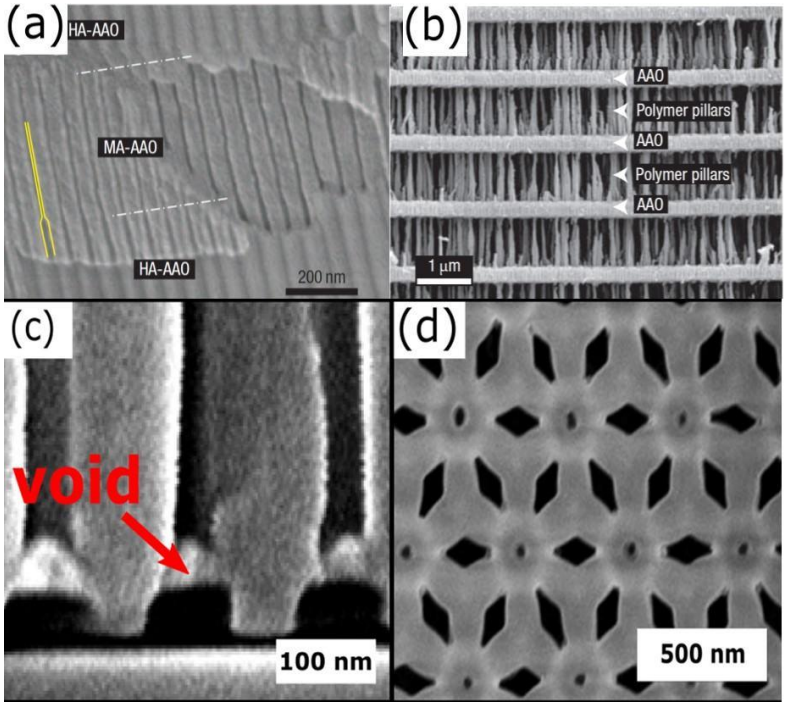

Fig. 13. SEM image showing a) the cross section view of as-prepared AAO produced by H_2SO_4 pulsed anodization, b) polymer nanopillars/AAO composite microstructure, with the MA/AAO slabs supported by PS nanopillars (Reproduced from Lee et al. 2008); (c) cross-sectional SEM image of the edge profile of pore bottoms that becomes angular with void growth by further anodization (Reproduced from Seo et al. 2007) d) FESEM image of diamond pattern obtained after etching of alumina template nanoimprinted pattern in aluminium Reproduced from Smith et al. (2008).

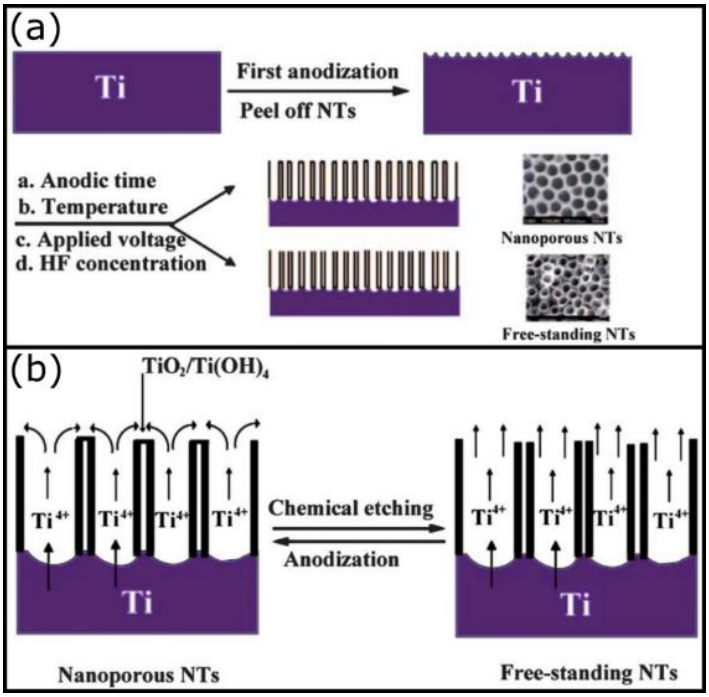

Fig. 14. Schematic diagram of: a) controllable fabrication processes and b) possible formation mechanisms of TiO_2 nanotubes (NTs) and nanopores. Reproduced from Yan and Zhou (2011).

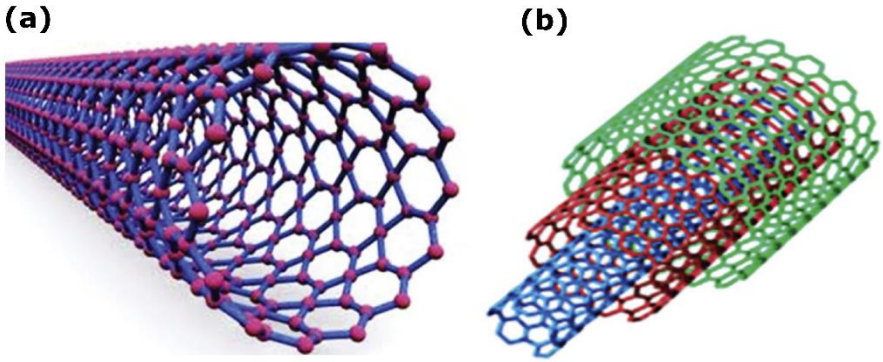

Fig. 15. (a) SWCNT, (b) MWCNT. Reproduced from Wang et al. (2014).

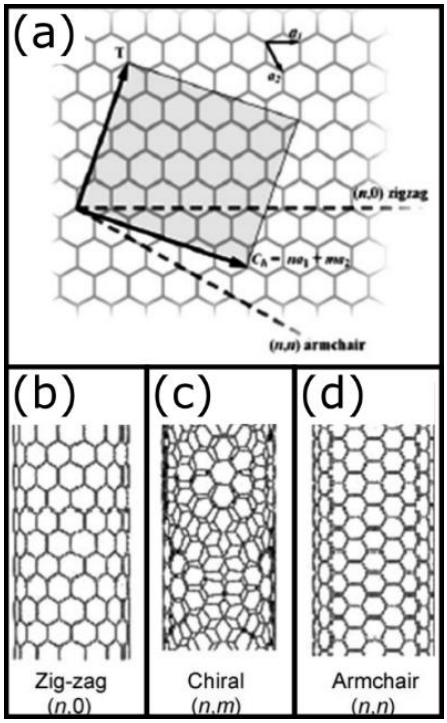

Fig. 16. Schematic diagram showing different CNTs structures. Reproduced from Zhang and Zhao (2009).

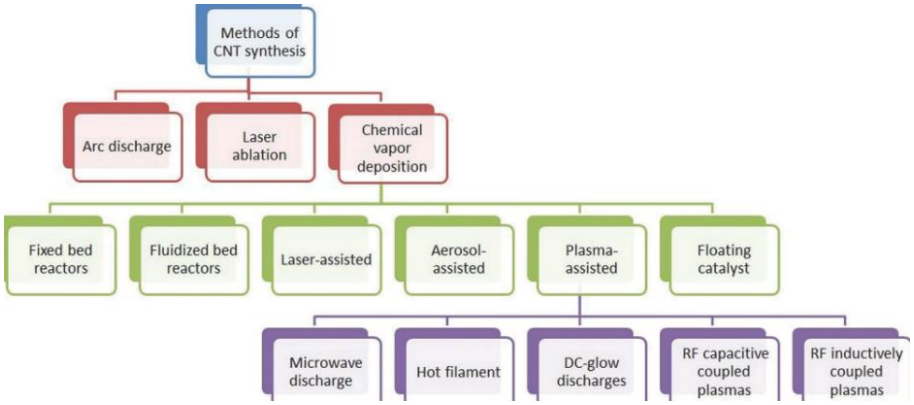

Fig. 17. Classification of CNTs manufacturing methods. Reproduced from Kumar et al. (2017).

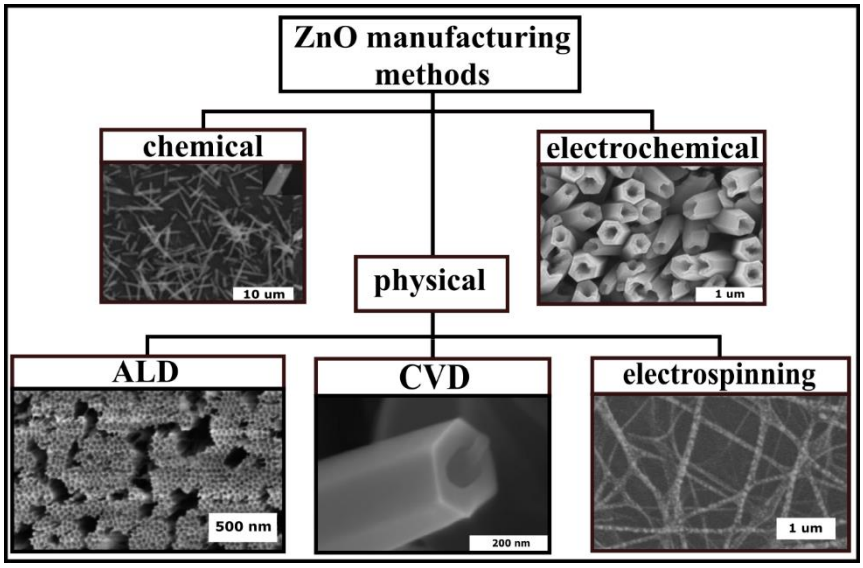

Fig. 18. The classification of ZnO NTs synthesis methods. Reproduced from (Samadipakchin et al. (2017), Long et al. (2019), Choi and Chang (2018), Zhang et al. 2015, Zhang et al. (2019).

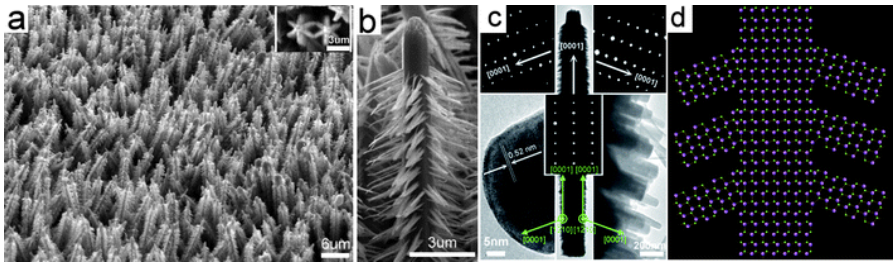

Fig. 19 (a) SEM image of typical branched ZnO nanotrees, (b) An enlargement of a side-view single nanotree, (c) TEM image of a single ZnO tree (middle) recorded along the [1210] selected-area electron diffraction patterns (top left, top right and centre) taken respectively from the branches and the trunk and lattice image (bottom left) and high-magnification TEM image (bottom right) of the branches. The green arrows indicate the major growth directions of the trunk and the branch, which share the [1210] direction. (d) A simple structural model of a branched ZnO nanotree projected along the [1210] direction. Relaxation at the interface between the trunk and the branch to achieve minimum interface energy is ignored here. Reproduced from Zhao et al. (2010).

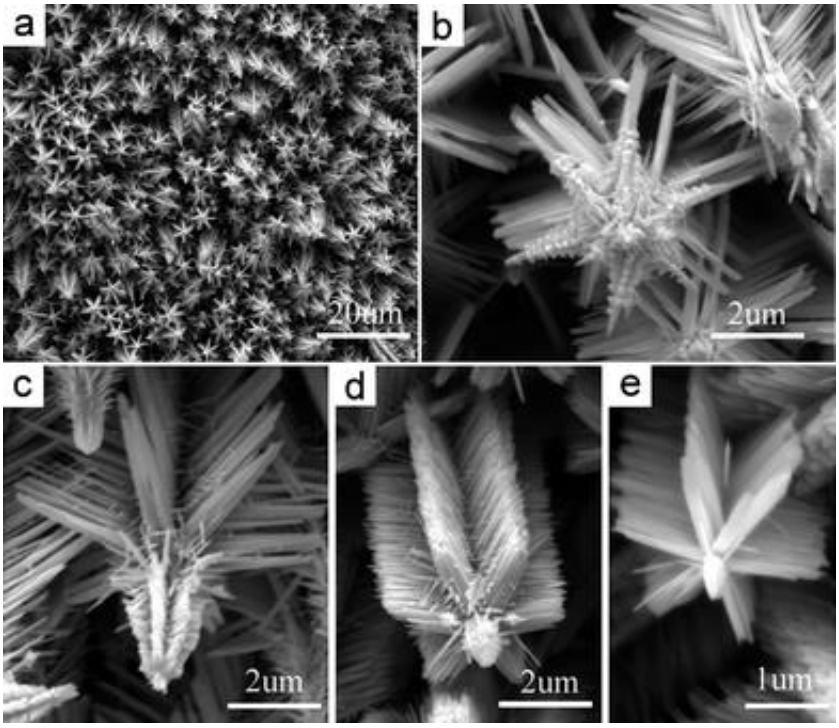

Fig. 20 SEM images show (a) the top-view of a complex ZnO array grown at 100°C with a concentration of 3.75 mol L^{-1} and (b)-(e) several unique individual ZnO crystalline trees. Reproduced from Zhao et al. (2010)

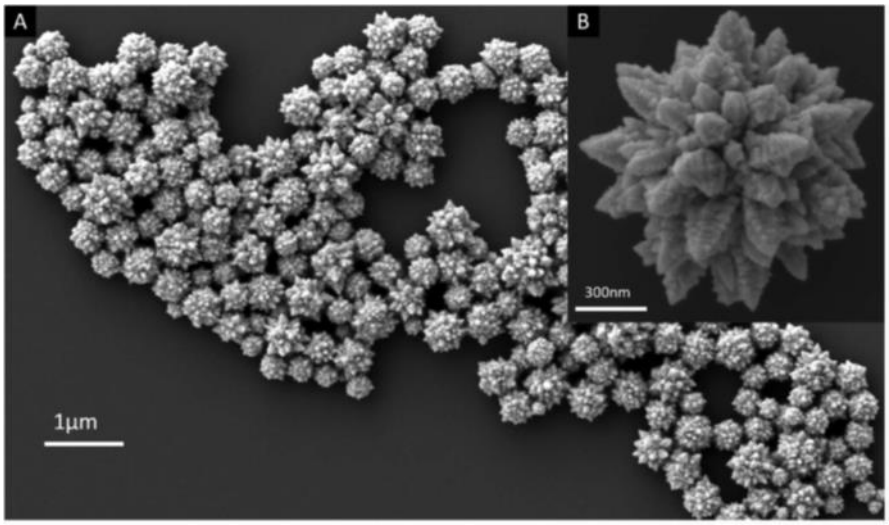

Fig. 21. a) SEM image of nanoflowers synthesized by reducing $HAuCl_4$ with dopamine. b) Inset presents morphology of a single flower. Reproduced from Yi et al. (2013).

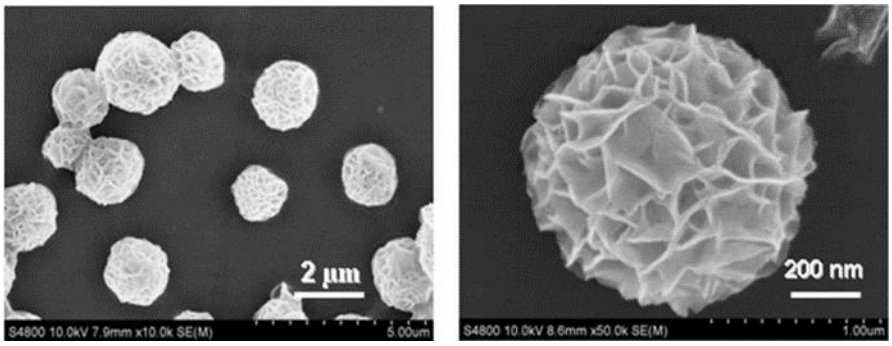

Fig. 22. DNA-based nanoflowers created with RCR method. Reproduced from Hu et al. (2014)

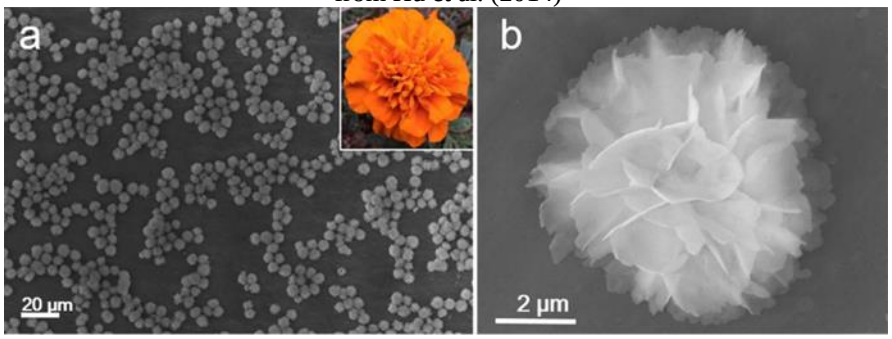

Fig. 23. Hybrid protein-inorganic nanoflowers synthesized using one-pot protocol. Reproduced from Liu et al. (2017).

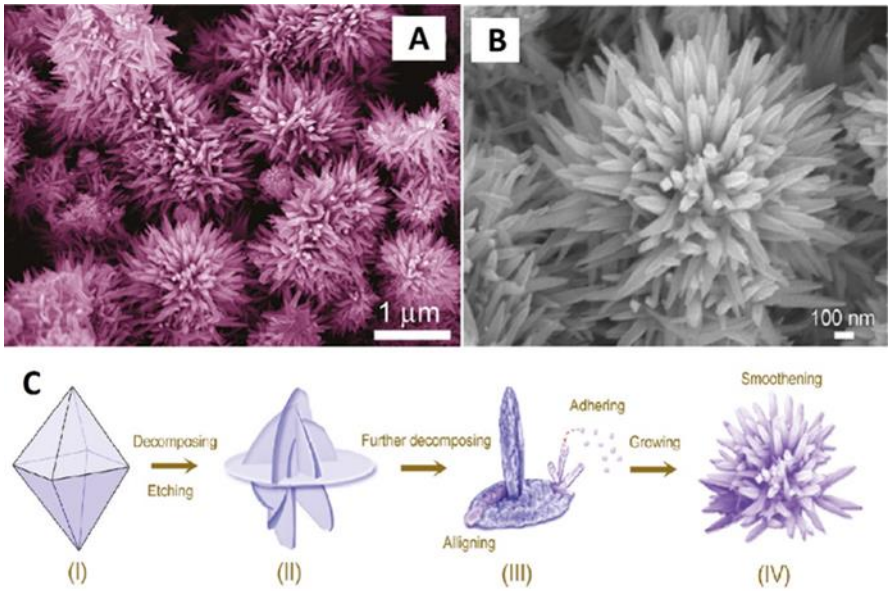

Fig. 24. a, b) SEM images of urchin-like nanostructures and c) schematic representation of the stages of their synthesis. Reproduced from Dou et al. (2011).

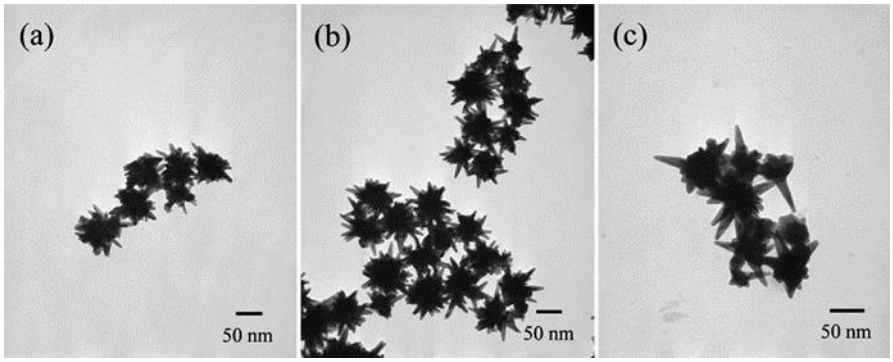

Fig. 25. AuAg nanourchin particles synthesized using different molar ratios of $HAuCl_4$: $AgNO_3$ - 3, 10, 15 for a), b) and c) consequently. Reproduced from Cheng et al. (2012).

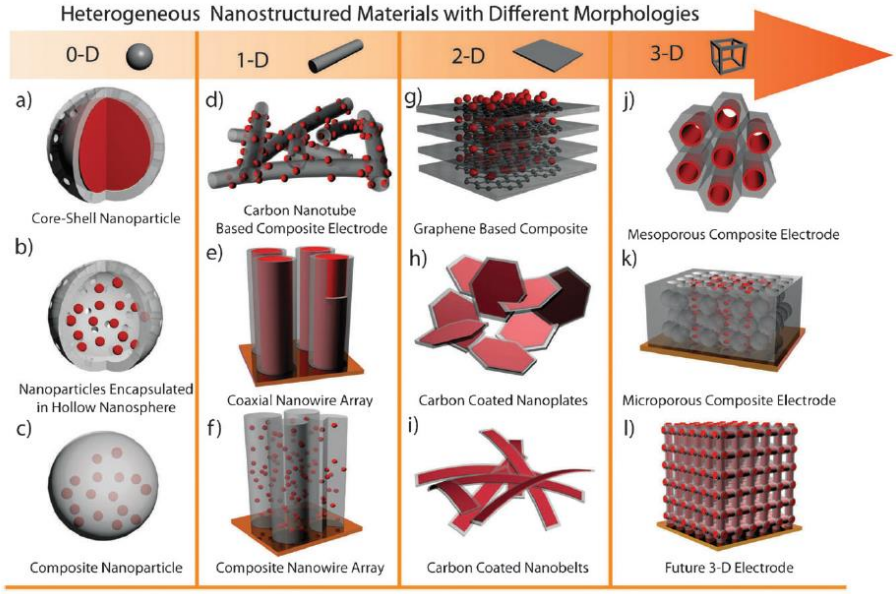

Fig. 26. Exemplary hybrid materials based on different structure configuration. Reproduced from Liu and Duay et al. (2011).

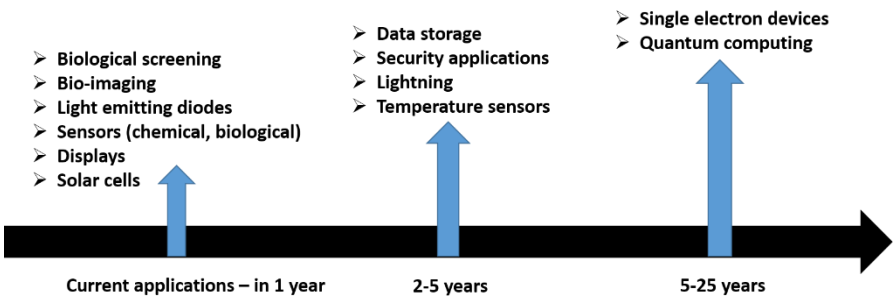

Fig. 27. Possible application of QD.

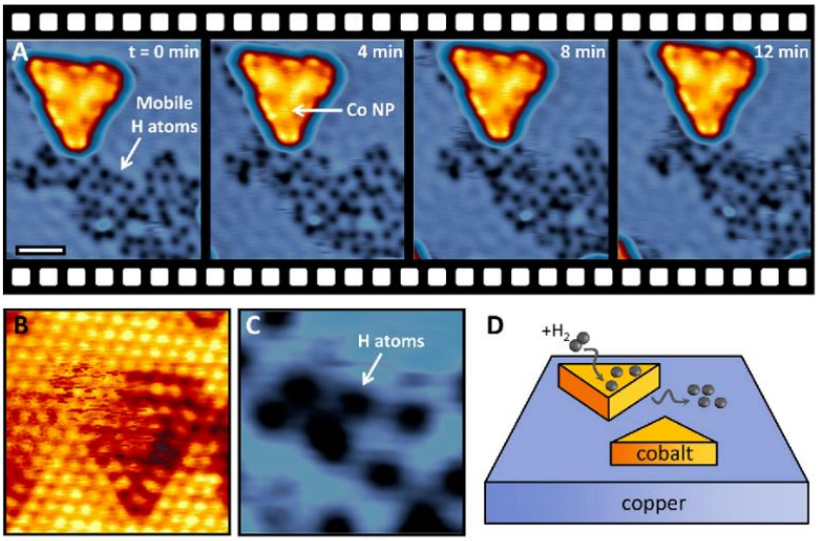

Fig. 28. Heterostructure composed of Co nanotriangles over Cu coating. Reproduced from Lewis et al. (2014).

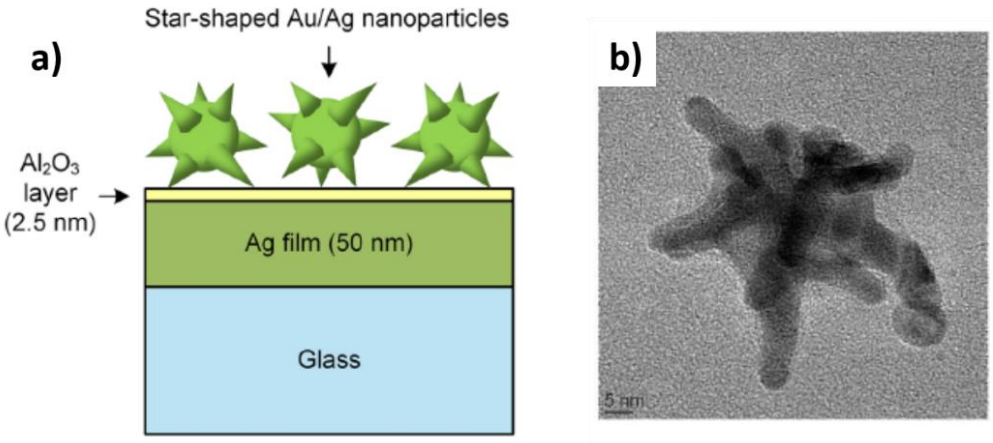

Fig. 29. a) Schematic of star-shaped nanoparticle based SERS substrate. b) TEM image of a single Au/Ag nanoparticle. Reproduced from Lai et al. (2017).

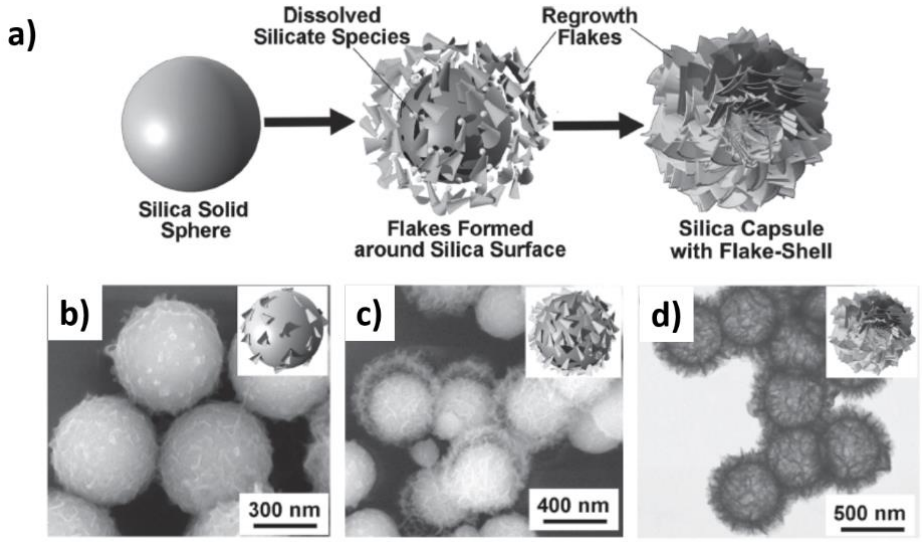

Fig. 30. a) Scheme of the formation route of flake-shell silica structures. b-d) SEM images of silica spheres overgrown by nanosheets. Reproduced from Ji et al. (2012).

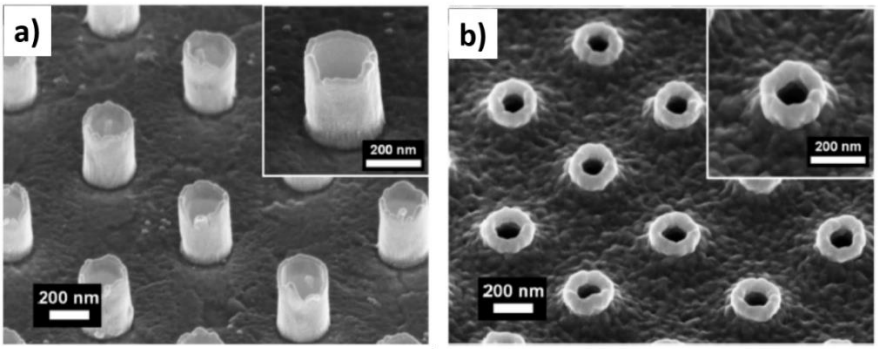

Fig. 31. SEM images of: a) 3-D hybrid nanostructure on ITO and b) the same nanostructure coated with polymeric material. Reproduced from Kim et al. (2017).

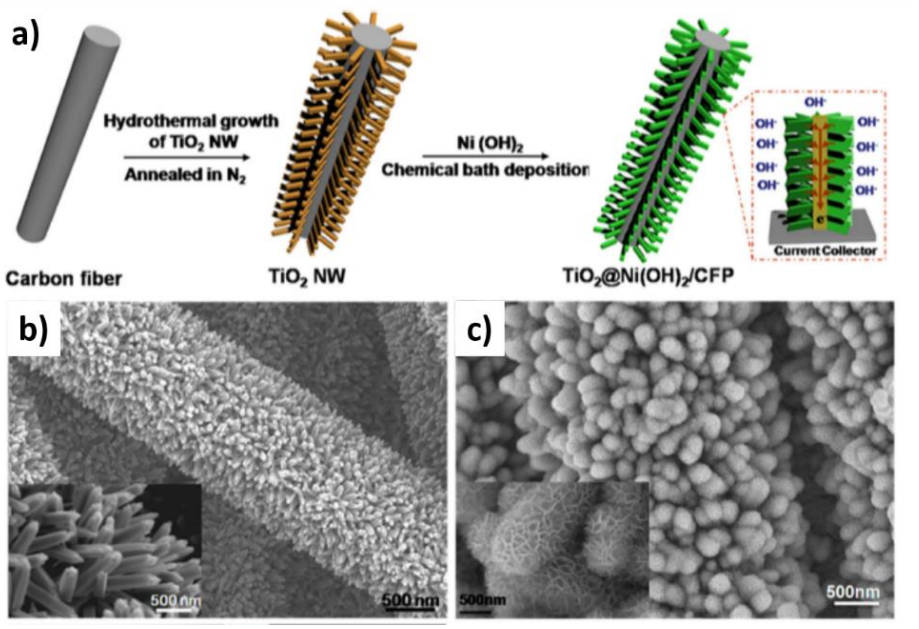

Fig. 32. a) Scheme of fabrication process of TiO_2@$Ni(OH)_2$ core-shell nanowire arrays onto carbon fiber paper (CFP). SEM images of: b) TiO_2 nanowire array and c) 3-D hybrid material. Insets: magnified images. Reproduced from Ke et al. (2015).

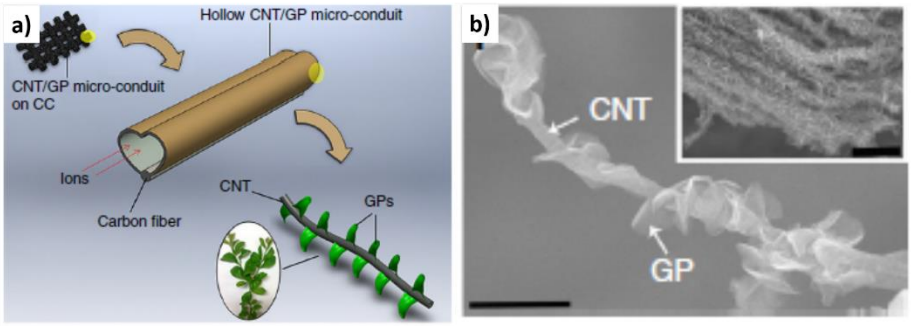

Fig. 33. a) Schematic illustration of 3-D heteromaterial. b) SEM image of carbon nanotubes covered with gold nanoparticles (GPs). Reproduced from Xiong et al. (2018).

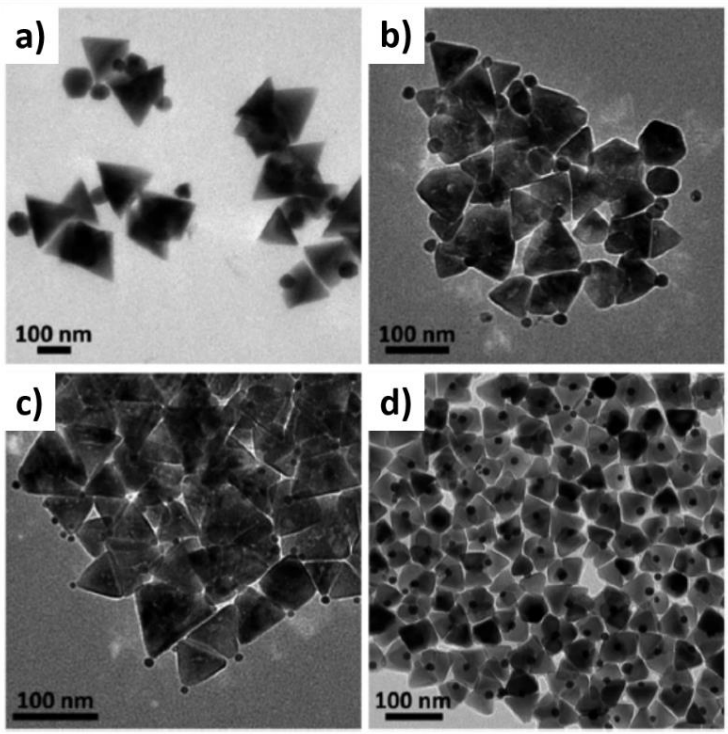

Fig. 34. TEM images of ZnO nanopyramid structures combined with different metallic nanoparticles: a) base-attached Cu, b) tip-attached Cu, c) Ag and d) Au. Reproduced from Flomin et al. (2014).

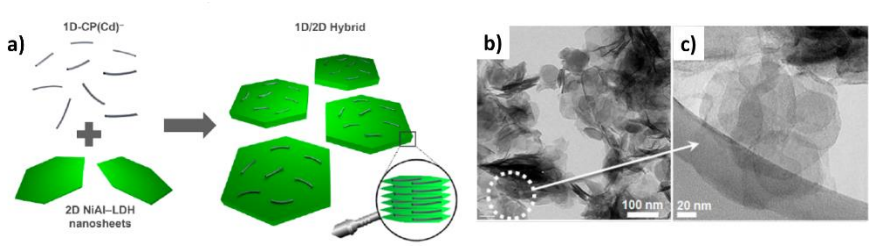

Fig. 35. a) Illustration of 1-D/2-D hybrid material preparation and its TEM image (b), c) Magnification of b). Reproduced from Abellan et al. (2016).